Nanoscale Advances

ROYAL SOCIETY OF CHEMISTRY

REVIEW

View Article Online
View Journal | View Issue

Cite this: *Nanoscale Adv.*, 2025, **7**, 4510

Electromagnetic interference shielding: a comprehensive review of materials, mechanisms, and applications

Hareesh M. S.,[a] Praveen Joseph[b] and Sumesh George *[c]

Rapid advancements in nanotechnology have led to electronic devices with densely integrated components, contributing to increased Electromagnetic Interference (EMI) pollution. EMI, a high-frequency electromagnetic signal, disrupts electronic circuits and can originate from external devices or within the affected component itself. Beyond causing electronic malfunctions, EMI exposure leads to health risks. This review discusses the Electromagnetic Interference Shielding (EMIS) mechanisms, such as reflection, absorption, and multiple reflection. It also examines recent advancements in EMIS materials, based on carbon-based, polymer-based, and carbon–polymer hybrid nanocomposites. It also investigates carbon-based materials, carbon nanotubes, graphene, and activated carbon due to their high electrical conductivity and EMI absorption properties. Polymer-based composites, incorporated with conductive polymers and metal oxides, are evaluated for their flexibility and processability. Carbon–polymer hybrid nanocomposites are highlighted due to their synergistic effects, combining the strengths of both components to achieve a high EMIS performance. This review also addresses the materials that are sustainable and recyclable for EMIS applications.

Received 13th March 2025
Accepted 20th May 2025

DOI: 10.1039/d5na00240k

rsc.li/nanoscale-advances

Introduction

EMI has emerged as a significant challenge in today's developing complex electronic landscape, which leads to signal degradation, data loss, and catastrophic failure of electronic devices and systems.[1] As the number of wireless communication systems, high-speed electronics, and internet-of-things (IoT) devices continues to grow, the need for effective electromagnetic shielding solutions has become inevitable.[2] Electromagnetic shielding is a crucial technique for mitigating EMI and leverages radio waves and matter interactions to create a protective barrier.[3] Various shielding methods, including conductive and magnetic materials, and innovative design principles, such as Faraday cages, have been developed to

[a]*St. Joseph's College of Engineering and Technology, Palai, India*
[b]*St. Joseph's College (Autonomous), Moolamattom, India*
[c]*Research and Postgraduate Department of Physics, St. George's College Aruvithura, India. E-mail: sumesh@sgcaruvithura.ac.in*

Hareesh M. S.

Hareesh M. S. is an Assistant Professor in the Department of Science & Humanities at St. Joseph's College of Engineering and Technology, Palai, with a total teaching experience of 14 years. He is currently conducting research in materials science, with a focus on microwave dielectrics, electromagnetic interference (EMI) shielding, and related areas.

Praveen Joseph

Dr Praveen Joseph is an assistant professor in the department of Physics, St Joseph's College, Moolamattom and also a research supervisor in physics at Mahatma Gandhi University, Kottayam, Kerala. He was conferred his PhD degree in Physics from Mangalore University and has 18 years of research experience. He has published 20 research articles in National and international journals and presented 21 articles in National and international conferences. He is a life member of the Academy of Physics Teachers, Kerala.

mitigate EMI. However, the effectiveness of these shielding techniques will depend on many factors, including wave frequency, strength, and material characteristics.[4]

This review thoroughly overviews the current advancements in electromagnetic shielding techniques and their underlying principles, benefits, limitations, and practical applications. This review mainly focuses on three primary categories of EMIS shielding materials: carbon-based,[5] polymer-based,[6] and carbon–polymer hybrid nanocomposites.[7] Carbon-based metal composites, including carbon nanotubes (CNTs), graphene, and activated carbon,[8] have attracted considerable interest because of their outstanding electrical conductivity and ability to absorb electromagnetic radiation.[9] These materials offer lightweight solutions with high shielding effectiveness (SE), which is ideal for making portable electronics and aerospace applications.[10] Polymer-based composites are widely used for EMIS shielding, which offers a combination of the flexibility and ease of processing of polymers with fillers having different conductive or magnetic properties.[11] Examples of this category include conductive polymers like polyaniline (PANI) and polypyrrole (PPy), as well as polymer matrices incorporating metal oxides and other nanoparticles. Thus, carbon–polymer hybrid nanocomposites represent a promising approach to EMIS, which leverages the synergistic effects of carbon materials and polymers. These hybrid materials typically demonstrate enhanced mechanical properties, greater thermal stability, and superior EMIS shielding performance compared to their individual components.[12]

This review aims to comprehensively analyse recent advancements in these three categories of EMIS materials by discussing their fabrication methods, characterization techniques, and shielding performance.[13] Additionally, the growing interest in sustainable and recyclable materials for EMIS applications will be addressed by highlighting the potential for environmentally friendly solutions in this field.[14]

Sumesh George

Dr Sumesh George is working as an Associate Professor and Research Guide in the Research and Postgraduate department of Physics, St. Georges College Aruvithura. He has 20 years of research experience and his PhD is from NIIST-CSIR Thiruvananthapuram. He did his postdoctoral research at the University of Kolkata and also the University of Nova Gorica, Slovenia, Europe. He contributed two chapters of a book published by Nova publishers UK and Elsevier Publishers. He has 25 research publications in reputed international journals and delivered talks at national and international conferences. He was the recipient of "Young Scientist award" in Kerala Science Congress 2009 and is a reviewer for many international journals. His research interests include microwave dielectrics, microwave antennas, EMI shielding, LTCC, etc.

EMIS mechanisms

EMIS mechanisms include reflection loss (SE_R),[15] absorption loss (SE_A)[16] and multiple internal reflection loss (SE_M).[17]

Reflection loss (SE_R). In shielding EMIS, reflection loss occurs due to the impedance mismatch between the incoming electromagnetic waves and the shielding material.[15] Due to their excellent electrical and thermal conductivity, metals are widely used in EMIS shielding.[18] High-permeability alloys, such as mumetal (comprising iron, copper, chromium, and nickel), are commonly used for shields and enclosures.[19] Other materials used for shielding include brass, aluminum, silver, nickel, stainless steel, metalized plastics, and conductive composites such as carbon and graphite.[20] However, these materials have drawbacks, such as carbon/graphite being fragile, aluminium lacking impact resistance, and stainless steel being heavy and subject to corrosion, particularly in marine environments.[21] The extent of reflection loss under plane wave (far-field) conditions can be described as,[4,22]

$$SE_R(dB) = -10 \log_{10}\left(\frac{\sigma_T}{16\omega\varepsilon_0\mu_r}\right) \quad (1)$$

In this equation, σ_T represents the total conductivity, ω represents angular frequency, f denotes the frequency measured in Hz, ε_0 denotes the permittivity of free space, and μ_r indicates the relative permeability with respect to free space.

Absorption loss (SE_A). Absorption loss (SE_A) is determined by the physical properties of the shielding material and remains unaffected by the type of source field. When an electromagnetic wave travels through a material, its amplitude decreases exponentially.[23] One skin depth of absorption loss is roughly 9 dB for a shield. At low frequencies, the skin effect becomes particularly significant, with magnetic fields predominating and wave impedance dropping below 377 Ω.[24] Effective shielding materials require a combination of high conductivity, high permeability, and sufficient thickness to achieve the necessary skin depths at the lowest frequency of interest, thereby ensuring adequate absorption loss.[25]

As an electromagnetic wave traverses a medium, its magnitude diminishes exponentially. This attenuation or absorption loss is a result of induced currents in the medium generating ohmic losses and material heating. The variables E_t and H_t can be represented as $E_t = E_i e^{-t/\delta}$ and $H_t = H_i e^{-t/\delta}$.[26] Now, the magnitude of the absorption term (SE_A) in decibels (dB) can be represented as[27]

$$SE_A(dB) = -20\ \frac{t}{\delta}\log_{10} e = -8.68\left(\frac{t}{\delta}\right) = -8.68t\left(\frac{\sigma_T\omega\mu_r}{2}\right)^{\frac{1}{2}} \quad (2)$$

In this equation, t represents the shield thickness measured in inches, while f denotes the frequency in Hertz. The formula demonstrates that SE_A is directly related to the square root of the product of the shield material's permeability (μ_r) and conductivity (σ_T).[25]

Multiple internal reflection loss (SE_M). The factor SE_M can be either positive or negative mathematically (though it is always negative in practice) and becomes negligible when the absorption loss SE_A exceeds 10 dB.[4] It is primarily significant for thin

metals at low frequencies, typically below around 20 kHz. The expression for the factor SE_M is given as follows[27]

$$SE_M(dB) = 20\log_{10}\left(1 - e^{-2t/\delta}\right) = 20\log_{10}\left|1 - 10^{\frac{-SE_A}{10}}\right| \quad (3)$$

SE_M is also relevant for porous structures, specific types of filled composites, or certain design geometries. However, it can be disregarded for a thick absorbing shield due to the high SE_A value, which reduces the amplitude of the wave to negligible levels by the time it reaches the second boundary.[28]

SE_M is primarily relevant for thin metals, porous structures, specific types of filled composites, or certain design geometries.[29] However, it can be disregarded for a thick absorbing shield due to its high SE_A value, which reduces the amplitude of the wave to negligible levels by the time it reaches the second boundary.[30] Recent advances have indicated that in addition to the multiple internal reflections, multiple external reflections can also contribute to the overall EMIS mechanism.[31] The combination of these multiple reflection processes, both internal and external, can lead to enhanced shielding effectiveness by trapping and attenuating the incident electromagnetic waves through repeated reflections within the composite structure.[32]

EMIS phenomenon: mathematical expressions

Theoretical EMIS efficiency. Eqn (4)–(6) are used to compute the ratio between incident and transmitted field strengths.[33]

$$SE_P = 10\log(P_{in}/P_{out}) \quad (4)$$

$$SE_E = 20\log(E_{in}/E_{out}) \quad (5)$$

$$SE_H = 20\log(H_{in}/H_{out}) \quad (6)$$

Here, P, E, and H represent the strength of the plane wave, electric field, and magnetic field of the electromagnetic wave, respectively. The subscripts "in" and "out" indicate the field strength that is incident on the surface and transmitted through the EMIS material. The SE is measured in decibels (dB).[16]

The overall shielding effectiveness (SE_T) of an EMIS material is the sum of three components:[13] SE due to absorption (SE_A), reflection (SE_R), and multiple internal reflections (SE_M), as illustrated in eqn (7).[16,34]

$$SE_T = SE_A + SE_R + SE_M \quad (7)$$

The SE_T of an EMIS material arises from the three mechanisms, with the skin depth shown in Fig. 1.[16]

The losses resulting from reflection and multiple internal reflection mechanisms are influenced by impedance, which will vary for the electric field, magnetic field, and plane wave.[35]

Experimental EMIS efficiency. To ensure comparable EMI shielding effectiveness across carbon-based, polymer-based, and carbon–polymer-based composites, standardized testing protocols like the coaxial transmission line method (ASTM D3637) and shielded box method are recommended.[36] The coaxial transmission line method is particularly useful for characterizing the

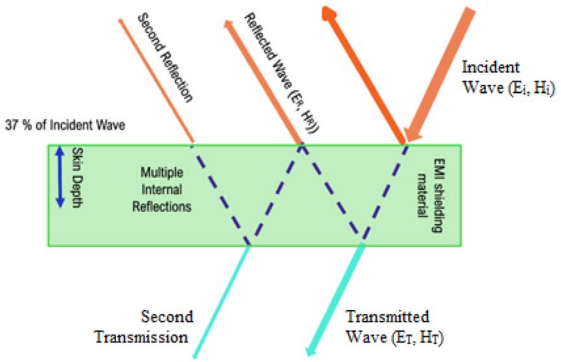

Fig. 1 The EMIS mechanism and the skin depth of a shielding material.

reflected, absorbed, and transmitted components of EMI shielding, while the shielded box method is suitable for lower frequency tests.[37] Open-field or free-space tests can also be used, but they are more suitable for testing finished products rather than characterizing individual materials. The coaxial transmission line method involves mounting the sample in a coaxial transmission line and measuring the scattering parameters (S-parameters) using a vector network analyser (VNA).[38] The VNA analyses the incident, reflected, and transmitted waves to determine the EMI SE. It can be resolved into its reflection, absorption, and transmission components, providing comprehensive characterization of the shielding performance of the material. This method is typically useful for characterizing the performance of planar materials and for evaluating the shielding effectiveness of materials at different frequencies.

EMIS is measured experimentally using devices called network analyzers. In a two-port vector network analyzer (VNA), the incident and transmitted waves are mathematically described using complex scattering parameters, also known as S-parameters, which are given by S_{11} (or S_{22}) and S_{12} (or S_{21}), respectively. They are correlated with reflectance (R) and transmittance (T) as $R = |E_R/E_I|^2 = |S_{11}|^2 = |S_{22}|^2$, $T = |E_T/E_I|^2 = |S_{12}|^2 = |S_{21}|^2$, which gives the absorbance (A) as[39]

$$A = (1 - R - T) \quad (8)$$

When SE_A exceeds 10 dB, SE_M becomes insignificant and can be disregarded. Therefore, SE_T can be represented as $SE_T = SE_R + SE_A$. Additionally, the intensity of the electromagnetic wave inside the shield after the initial reflection is determined by the factor $(1 - R)$. This factor is then used to normalize the absorbance (A) to calculate the effective absorbance.

$$A_{eff} = [(1 - R - T)/(1 - R)] \quad (9)$$

Fig. 2 shows the S-parameters generated from a two-port vector network analyzer (the VNA), which represent incident and transmitted electromagnetic waves.[36]

So, experimental reflection and absorption losses can be expressed as[40]

$$SE_R = 10\log_{10}(1 - R) \quad (10)$$

Fig. 2 Complex scattering parameters of an EMIS material from a two-port VNA.

$$SE_A = 10\log_{10}(1 - A_{eff}) = 10\log_{10}\frac{T}{(1-R)} \quad (11)$$

Categories of materials for EMIS

To achieve optimal EMIS, a harmonious blend of electrical conductivity (σ), magnetic permeability (μ), dielectric permittivity (ε), and structural features (*e.g.*, porous architecture) is essential. This combination facilitates losses *via* reflection, absorption, and multiple reflections. Metals, renowned for their superior electrical conductivity, remain the primary choice for EMIS materials.[25] Nevertheless, these materials face challenges, including high reflectivity, susceptibility to corrosion, increased weight, and costly production processes. Given these drawbacks, polymer-based composites and blends have emerged as promising alternatives. These materials have gained attention due to their unique combination of properties including electrical, thermal, dielectric, magnetic, and mechanical characteristics,[41] which contribute to their efficacy in electromagnetic shielding applications.[13] As a result, in recent times, numerous polymer composites have been created for electromagnetic shielding purposes by using diverse fillers such as conducting polymers, carbon nanotubes (CNTs), graphene-based materials,[41] and MXenes incorporated with polymer matrices.

Carbon-based nanocomposites

Carbonyl iron@SiO_2/Ni@Ag/silicone rubber composite film. T. Chen *et al.*[5] presented a novel approach for creating ultralow-reflection EMIS composite films. Their method involves the controlled alignment of carbonyl iron@SiO_2 (CS) and Ni@Ag (NA) microparticles within silicone rubber, which is achieved through magnetic manipulation. They developed flexible, multi-layer, absorption-dominant shielding materials (SRMs), with carbonyl iron chosen for its strong magnetization and scalability by using magnetic alignment.[42]

The researchers created CS microparticles using various precursor ratios to develop a highly structured absorption layer, followed by the alignment of NA microparticles to make the composite film (CSNA). The film demonstrated outstanding mechanical properties, enhanced flexibility, and very low electromagnetic wave reflection due to its absorption, reflection, and reabsorption mechanism. When unstretched, it shows an effective EMIS of 64.5 dB with minimal reflection ($R = 0.044$). It retained a substantial shielding of 38.6 dB even under 100% strain, showing promise for applications like wearable electronics and morphing aircraft sealing. The mechanical properties of the CSNA film were assessed at room temperature using a universal testing machine set to a constant speed of 50 mm min^{-1}. Meanwhile, the electrical conductivity of the CSNA composite film was measured with multi-point probe resistivity testing equipment.[5]

The SE values of carbon composites like carbon nanotubes (CNTs) with polyurethane (PU), silicone rubber/silver (Ag) and silicone rubber (SR), coating of the carbon nanofiber@cobalt (Co@CNF), and polypropylene are given in Table 1.

Cellulose nanofiber composites. Asymmetric multilayer cellulose nanofiber composite membranes with dual-gradient electrical and magnetic architectures for superior EMIS performance present a sustainable and effective method to address electromagnetic pollution in portable devices by developing asymmetric multilayer EMIS membranes.[48] Advances in EMIS materials have explored different structural designs, including porous,[49] fibrous,[50] and multilayer structures,[51] with multilayer structures standing out for their thin profiles and high shielding efficiency.[52]

Y. Zhou *et al.* highlighted the importance of structural design strategies in MXene-based nanocomposites for EMIS applications.[48] In this study, new asymmetric multilayered composite membranes composed of cellulose nanofiber/multiwalled carbon nanotube@ferroferric oxide/MXene (CNF/MWCNT@Fe_3O_4/MXene)[53] with electrical-magnetic dual-gradient structures were fabricated using a layer-by-layer self-assembly approach.[54]

In brief, the CNF/MWCNT@Fe_3O_4 layers serve as negative gradient absorption layers, allowing for both dielectric and magnetic loss.[55] At the same time, the MXene layers function as positive gradient reflection layers, which produce multiple reflections and contribute to conductive loss. As a result, the

Table 1 SE values of different carbon composites

No.	Composite materials	Processing method	Thickness (mm)	SE (dB)	Frequency range (GHz)	References
1	CSNA film	Magnetic alignment	1.6	64.5	8.2–12.4	5
2	Graphene/PU	Hydrothermal	1.5	61	8.2–12.4	43
3	Ag/Fe_3O_4@MWCNT/SR	Supercritical carbon dioxide foaming	0.7	30.5	8.2–12.4	44
4	MXene/Fe_3O_4/SR (SRMF)	Vacuum-assisted dipping and curing	—	55.5	8.2–12.4	45
5	Co@CNF	Hydrolysate of waste leather scraps	0.25	49	8.2–12.4	46
6	CNT/polypropylene	Latex mixing and template foaming	2.2	48.3	8.2–12.4	47

gradient multilayered CNF/MWCNT@Fe_3O_4/MXene composite membranes show an SE_T of 73.20 dB at a layer thickness of 180 μm and an *R*-value of 0.99934 in the X-band.[48]

Moreover, the asymmetric gradient multilayer composite membrane shows significantly better EMIS performance compared to homogeneous multilayered composite membranes.[51] As electromagnetic waves (EMWs) pass through the gradient multilayered CNF/MWCNT@Fe_3O_4/MXene composite membrane, the carefully designed asymmetric gradient multilayered structures facilitate a shielding mechanism of "gradually decreasing absorption and gradually increasing reflection".[48,55,56] Thus, the design strategy of asymmetric electrical-magnetic dual-gradient structures proves beneficial in improving the EMIS performance of polymeric composites.[57]

The asymmetric design surpassed uniform multilayer membranes by utilizing a unique "gradually decreasing absorption and gradually increasing reflection" mechanism, combined with magneto-electric synergy, to improve SE.[48] While the study acknowledges issues like MXene oxidation and membrane brittleness, further research is recommended to enhance CNF/MXene composites for real-world applications. Despite these obstacles, the study highlights a promising pathway for advancing thin, flexible, high-performance EMIS materials. SE of MXene-based composites is shown in Table 2.

3D carbon nanotubes/graphene aerogel films. Recent advancements in fabricating graphene into 3D structures have garnered significant attention for preventing graphene nanoparticle aggregation and achieving high EMIS SE, making them ideal for lightweight shielding applications.[61–63] However, conventional methods for producing 3D graphene often involve high temperatures[64,65] or harmful chemicals[66] or annealing processes[67,68] that are not eco-friendly. A key issue with 3D graphene is that surface defects and incomplete network formation can limit its EMI SE. To overcome this, incorporating CNTs into graphene through π–π interaction can improve conductivity and enhance EMI SE.[62,69]

H. Liu *et al.*[9] built on prior work with a 3D CNTs/Graphene Aerogel Film (CGAF) created through a green reduction method,[62] comparing its EMI shielding efficiency (EMI SE) to theoretical predictions and investigating how its 3D leaf-like structure contributes to EMIS. The inclusion of vein-like CNTs improved conductive pathways, increasing the total SE by 5.1 dB. While compressing CGAF into C5GP slightly reduced SE, the 3D structure enhanced electromagnetic wave absorption through repeated reflections. The study underscores the benefits of 3D-structured composites in boosting EMI SE, particularly in absorption, making them ideal for applications requiring both lightweight and flexible materials. The SE of different carbon composites with multilayer CGAF and polydimethylsiloxane (PDMS), anisotropic polyimide (PI)/graphene composite aerogels, and carbon nanotube/graphene/polyimide foam (CGP) is shown in Table 3.

MWCNT/zinc-doped nickel ferrite nanocomposites. Carbon-based materials are renowned for their high permittivity to electromagnetic radiation, while ferrites exhibit high permeability driven by natural resonance and eddy currents, contributing to significant electromagnetic losses.[74–76] Spinel $Ni_{1-x}Zn_xFe_2O_4$ (NZF) is extensively utilized in electrical and magnetic applications across low and high-frequency ranges due to its excellent electromagnetic properties, low dielectric loss, high permeability, and high resistivity.[77–80]

Research by S. Tyagi *et al.*[81] demonstrates that microwave sintering of Ni–Zn ferrites enhances their magnetic properties while reducing dielectric values. Meanwhile, the dielectric conductivity of CNTs has been reported to range between 10^6 and 10^7 S m^{-1}.[82] M. Chahar *et al.*[80] used two synthesis techniques solid–state reaction or Physical Mix (PM) and co-precipitation or Chemical Mix (CM) to examine the electromagnetic properties of $Ni_{0.5}Zn_{0.5}$ Fe_2O_4/MWCNT

Table 2 SE values of different cellulose nanofibre composites

No.	Composite materials	Processing method	Thickness (mm)	SE (dB)	Frequency range (GHz)	References
1	CNF/MWCNT@Fe_3O_4/MXene	Vacuum filtration	0.18	73.2	8.2–12.4	48
2	CNF/MXene/AgNWs	Vacuum filtration	—	61.9	8.2–12.4	58
3	CNF@MXene@AgNW film	Vacuum-assisted filtration	—	55.9	8.2–12.4	59
4	CNF@MXene	Hot-press sintering	—	41.8	8.2–12.4	60
5	(CNF)@MXene	Vacuum filtration	0.035	40	8.2–12.4	54

Table 3 SE of different carbon 3D-structured CNT/graphene-based composites

No.	Composite materials	Processing method	Density	Thickness (mm)	Specific EMI SE	SE (dB)	Frequency range (GHz)	References
1	C5GAF	Green reduction method	0.0087 g cm^{-2}	0.012–0.014	12 091 dB cm^2 g^{-1}	74.7	8.2–12.4	9
2	CGF/PDMS	Chemical vapor deposition	12.5 mg cm^{-2}	—	1142 dB cm^3 g^{-1}	71.4	8.2–12.4	70
3	F-MG foam	Fluid-assisted method	0.011 g cm^{-3}	40	3410 dB cm^3 g^{-1}	37.2	8.2–12.4	71
4	PI/graphene aerogel	Unidirectional freezing	0.076 g cm^{-3}	—	1518 dB cm^2 g^{-1}	28.8	8.2–12.4	72
5	CGP foams	*In situ* polymerization	0.02 g cm^{-3}	—	7050 dB cm^2 g^{-1}	28.2	8.2–12.4	73

nanocomposites. In the solution mixing approach, functionalized MWCNTs were dispersed in 5 ml of xylene and subjected to ultrasonication for 1 hour. Similarly, nickel–zinc ferrite was dispersed in 10 ml of xylene and sonicated for 3 hours. Afterwards, the two solutions were combined and sonicated together for an additional 3 hours. The resulting mixture was dried in an oven at 70 °C and then ground using a mortar and pestle to obtain the $Ni_{0.5}Zn_{0.5}Fe_2O_4$/MWCNT nanocomposite (CM). In the physical mixing method, the ferrite and functionalized MWCNTs were combined in a 3 : 1 weight ratio and ground with a mortar and pestle for 4 hours to produce the composite material in powder form (PM), as shown in the schematic diagram in Fig. 3.[80]

The goal of the work[80] was to assess how hybridization affects electromagnetic parameters to optimize properties for high-frequency device applications. XRD confirmed the spinel structure of the NZF and NZF/MWCNT composites, and FESEM images showed a hexagonal flake-like structure with an average particle size of 23.1 nm, further validated by TEM. The energy band gap of NZF was 1.9 eV, reducing to 1.3 eV for PM and 1.1 eV for CM. The PM composite showed a lower dielectric constant than CM, with magnetic permeability (μ') ranging from 1.5 to 0.25, except for a negative value at 11.9 GHz in CM. CM also displayed a resonance peak in magnetic permeability (μ'') at 10.5 GHz, linked to domain wall motion.[83]

When electromagnetic (EM) radiation interacts with the sample, it undergoes reflection and transmission, as illustrated in Fig. 4. A portion of the incident radiation is absorbed, leading to a gradual reduction in intensity with each successive reflection. This reduction is caused by electric and magnetic losses in the material, where the energy of the electromagnetic wave is lost as hysteresis due to alternating electric and magnetic polarizations. This decrease in intensity, known as absorption loss, primarily stems from two factors: ohmic losses from currents induced within the material and losses associated with infrared radiation. At higher frequencies, the losses become dependent on frequency, with a notable increase at certain resonance frequencies, peaking at about 40.1 dB at 10.6 GHz.[84]

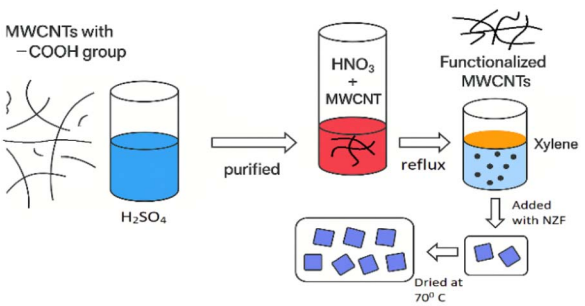

Fig. 3 Schematics of the synthesized MWCNTs/NZF nanoparticles.

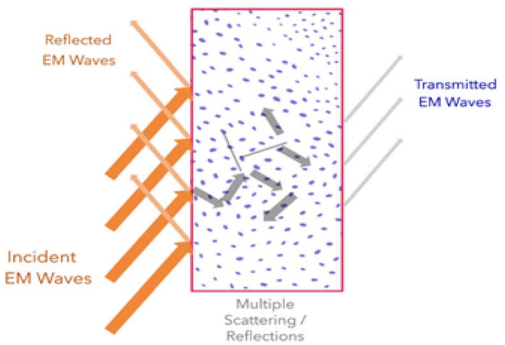

Fig. 4 The interaction of EM waves incident on any material.

The highest reflection loss (RL) of −51.2 dB was observed at 11.2 GHz with a 0.45 GHz bandwidth for PM, while CM demonstrated an SE_T of approximately 45.5 dB within the 8.2–12.4 GHz range for MWCNTs, as indicated in Table 4.

Carbon fiber felt @ nickel composite films. Conductive materials, such as the carbon-based materials, generate heat under applied voltages and have advantages such as cleanliness, silent operation, and wide usability.[93] However, the traditional metallic materials face challenges due to costs, difficult moulding, and processing. Recent research has revealed that heterostructures created with pre-established three-dimensional (3D) microelectrical networks in composites exhibit distinctive electrical behaviours over a nonconductive continuous phase.[94] Carbon fiber felt (CFF) is an ideal component for constructing heterostructures where both electrical conductivity and structural flexibility are essential. Nickel (Ni) exhibits excellent electrical and thermal conductivity and corrosion resistance properties, leading to a rational choice to design and create a heterostructure by decorating the CFF skeleton with Ni particles.[95]

Liu *et al.*[29] developed a novel flexible CFF@Ni composite film using an electroplating strategy. CFF@Ni-1.5 signifies the composite film fabricated by applying a current density of 1.5 A dm^{-2}. The film has a distinct core–shell heterostructure, with CFF as the core and interconnected Ni particles as the shell. This arrangement provides excellent electrothermal management and uniform surface heating properties. CFF@Ni can reach a maximum surface temperature of 146.7 °C with a low actuation voltage of 1.5 V at a heating rate of 35.8 °C s^{-1}. It also has an excellent heating–cooling stability during rapid testing cycles and long-term stability for 8 hours.

The CFF@Ni-1.5 shield shows a higher EMIS performance compared to CFF, with higher absorbing loss (SE_A) values than reflection loss (SE_R) values. It is due to the skin effect in the shallow near-surface region of a shield.[96] Multiple reflections at the internal interfaces increase overall shielding performance, resulting in improved SE_T.[30] The porous structure of CFF@Ni includes several internal interface areas for multiple reflections as well as a special dual 3D conductive network that combines the CFF skeleton and Ni coating layer.[31]

The different electrical characteristics of CFF and Ni particles cause multiple internal reflections, whereas the outside shell of the coating layer of Ni particles experiences multiple outward reflections.[32] As a result, the path of electromagnetic wave transmission is extended by effective multiple reflections. The closely stacked layer of Ni particles creates a limited 3D environment that is subject to constant reflection and re-

Table 4 Reflection loss values of different MWCNT-based composite materials

No.	Composite materials	Processing method	Thickness (mm)	Reflection loss (dB)	SE (dB)	Frequency range (GHz)	References
1	MWCNT/NZF (CM)	Chemical mixing	1.2	−45.5	40.1	8.2–12.4	80
2	MWCNT/NZF (PM)	Physical mixing	1.2	−51.2	45.2	8.2–12.4	80
3	NZF	Co-precipitation	1.2	−39.7	10.8	8.2–12.4	80
4	CNTs–$Ni_{0.5}Zn_{0.5}Fe_2O_4$	Precipitation-hydrothermal method	6	−32.5	—	2–12	85
5	MWCNT/$SrFe_{10}$ $(Sn_{0.5}$ $Zn_{0.5})_2O_{19}$	Co-precipitation	1.5	−29	—	8–12	86
6	$Cu_{0.25}Ni_{0.25}Zn_{0.5}Fe_2O_4$/ 0.16%-MWCNTs/epoxy	Co-precipitation	2.5	−37.7	—	8.2–12.2	87
7	MWCNTs/epoxy	Solution-mixing	2.5	−12.7	—	8.2–12.2	87
8	NZCF-1–CNT	Sol–gel method	2	−22	—	8–12	88
9	NZCF-2–CNT	Sol–gel method	2	−33	—	8–12	88
10	MWCNTs/$NiFe_2O_4$	Facile one-pot solvothermal strategy	1.2	−42.3	—	2–22	89
11	MWCNT/$Ni_{0.7}Zn_{0.3}Fe_2O_4$/GO	Sol–gel method	2.4	—	71.1	8.2–12.4	90
12	MWCNT/$Co_{0.7}Zn_{0.3}Fe_2O_4$/GO	Sol–gel method	2.4	—	81.6	8.2–12.4	90
13	MWCNT/Mn Zn ferrite/epoxy	Citrate gel method	2.0	—	44	8.2–12.4	91
14	Fe_3O_4/PPY/CNT	Co-precipitation	3.0	—	26	8.2–12.4	92

Table 5 EMIS performance of various heterostructure composite materials

No.	Composite materials	Processing method	Thickness (mm)	EMI SE (dB)	Frequency range (GHz)	References
1	WS_2–CF	Hydrothermal	3	36	2	31
2	BF/PANI	*In situ* polymerisation	0.4	37.72	8–12	30
3	PET/PANI	*In situ* polymerisation	0.29	23.95	8–12	32

reflection of incoming microwaves. This unique architecture effectively traps incident microwaves, resulting in an excellent EMI shielding capability. The EMI SE of different heterostructures like tungsten disulphide (WS_2)–carbon fiber (CF), natural bagasse fiber/polyaniline (BF/PANI) core–shell composites, and flexible polyethylene terephthalate/polyaniline (PET/PANI) composites is given in Table 5.

Polymer-based nanocomposites

PVA/POM hybrid nanocomposites. In recent years, the use of conductive micro/nanofillers in insulating or partially conductive polymer matrices has attracted considerable interest in creating electrically conductive polymer nanocomposites.[97] Due to their unique physical and chemical characteristics, these fillers are often divided into four categories: metallic, carbon-based, ceramic, and metal-oxide. Metal-oxide nanoparticles, such as Fe_2O_3, ZnO, and TiO_2, are of special interest.[98] Factors such as size, shape, structure, and crystalline nature significantly affect the performance of these metal oxide nanoparticles.[99] TiO_2 is especially noted for improving both the flexibility and performance of polymer matrices.[100] Polymer composites incorporating metal oxides with higher dielectric constants are emerging as viable materials for EMIS. This work adopts a cost-effective solution-casting approach to create hybrid nanocomposites by blending polyoxymethylene (POM) and polyvinyl alcohol (PVA) with varying concentrations of TiO_2 nanoparticles.[101]

To produce size-controlled TiO_2 nanoparticles, freshly prepared egg albumin was utilized as a bio-capping agent in a combustion method, which reduced nucleate agglomeration and allowed for precise morphology control compared to other chemical methods.[102] The process involved thoroughly mixing freshly prepared egg albumin with 0.2 M nitric acid under continuous stirring. $TiCl_4$ solution was then slowly added drop by drop while stirring being continued for about two hours at normal temperature. The mixture was then heated to 90 °C and simmered for nearly six hours, during which burning fumes indicated the reaction's completion. The resulting fluffy material was crushed to obtain the final TiO_2 nanoparticles.[6]

Previous research, including work by S. Patil *et al.*[101] and El Sayed and Morsi,[103] has shown that polymer blending can enhance mechanical, optical, and dielectric properties. M. E. Prince *et al.*[6] developed $PVA_{0.5}/POM_{0.5}$ blends with 1–4 wt% TiO_2 nanoparticles that were evaluated for their dielectric and shielding capabilities of 12 dB and 13 dB in the X band and Ku band, respectively, with 25 wt% TiO_2 NP loading.[38]

The PVA/POM nanocomposite films and tertiary nanocomposite films comprising poly styrenesulfonic acid (PSSA)/PVA with different TiO_2 NP loadings were studied using a Vector Network Analyzer with a waveguide dimension of 10 × 10 mm, and PVA/polyethylene glycol (PEG) blend nanocomposite films reinforced with various loadings of carbon black nanoparticle (CBNP) materials for EMI SE are shown in Table 6.[38]

Table 6 SE values of different PVA composite materials produced by the solvent casting method

No.	Composite materials	Weight (%)	Thickness (mm)	Reflection loss (dB)	Frequency range (GHz)	References
1	PVA/POM	TiO_2 (0)	4	2	8–12	6
2	PVA/PSSA	TiO_2 (25)	0.07	12	8–12	38
3	PVA/PSSA	TiO_2 (25)	0.07	13	12–18	38
4	PVA/PEG film	CBNP (25)	0.06–0.08	10.6	12–18	104
5	Polypyrrole/PVA	Ag (10)	4	−35	8–12	38

A 3D porous heterostructure with strong electromagnetic absorption characteristics was designed and fabricated by H. Gao *et al.*[94] using nickel metal foam (NF) as the framework. A PANI coating layer was applied to the NF framework using a simple *in situ* polymerization strategy. This created a Ni/PANI composite foam (NPF), with strong dielectric relaxation and strong interfacial polarization. The preparation process is efficient, cost-effective, and can be easily expanded for large-scale advanced shielding production. The NPF demonstrates extraordinary shielding ability up to 93.8 dB. The 3D porous heterostructure efficiently integrates multiple reflection, scattering, embedded interfacial polarizations, and low density, making it a promising candidate for next-generation or large-scale shielding systems. The prepared NPF can be easily extended to other metal foams to exploit high-performance metal foam/PANI shields.

Polyethylene terephthalate membrane. Recycled materials are increasingly being used in EMIS to promote environmental protection and resource conservation, including items like PET, iron (Fe), cobalt (Co), carbon (C), carbon fibres, and leather waste.[105,106] In particular, PET has been utilized in diverse fields such as bottles, textiles, and electronics due to its remarkable tensile strength, thermal stability, clarity, and resistance to chemicals.[107] A new multifunctional EMIS membrane made of recycled polyethylene terephthalate (rPET) with magnetic FeCo@C nanoparticles and highly conductive silver nanowires (Ag NWs)[108] is presented by Z. Jiang *et al.*[109] The quantity of Ag NWs on the surface increases with the Ag NW coating time from 30 minutes (Ag30) to 90 minutes (Ag90). To stabilize the coating particles and give the membrane surface superhydrophobicity, polydimethylsiloxane (PDMS) was dissolved in hexane and dip-coated onto it.[109]

A novel, flexible, and cost-effective EMI shielding composite paper has been developed by Y. Zang *et al.*[32] using a simple, efficient, and environmentally friendly *in situ* polymerisation process. The paper exhibits excellent shielding stability and outstanding bending durability, retaining 99.0% of its original value even after 10 000 times of bending. The composite paper can achieve a maximum shielding performance of 23.95 dB in the X-band, meeting commercial requirements. The thin FPP-4 paper has an efficient SE of up to 23.95 dB and outstanding shielding reliability under mechanical bending deformation. The dominant shielding mechanism is absorption. This approach could be applied to a wide range of flexible EMI shielding materials, making them potentially suitable for use in next-generation flexible devices.

Overall, this research highlights the potential of hybrid polymer nanocomposites to deliver superior electrical properties compared to single polymer matrices.

Despite having a tiny 12.33 μm conductive layer, it has an outstanding SE_T of 68 dB in the X band. The membrane also retains stable electrical conductivity. This combination of multifunctionality and sustainability positions the rPET/FeCo@C/Ag90/PDMS20 membrane as a promising material for future electronic applications. The EMIS performance of composites is shown in Table 7.[48]

Nacre-inspired starch-based bioplastics. According to Armynah *et al.*[113] and Dai *et al.*,[114] starch is frequently considered an optimal raw material for bioplastics due to its abundance, affordability, non-toxic nature, and biodegradability, although its limited mechanical properties and stability restrict its broader application. According to Zhang, Gao, *et al.*,[115] adding carbonaceous materials like reduced graphene oxide (rGO) can increase EMIS. Liu *et al.*[14,116] introduced a novel biomimetic starch-based bioplastic, SBP_{SCGM15}, featuring a nacre-like layered structure achieved through the self-assembly of TEMPO-CNF, starch, nano montmorillonite (NMMT), and rGO, which greatly enhances mechanical properties along with EMIS efficiency, offering a promising approach for future applications. Di Xie *et al.*[14] introduced an innovative method for developing a starch-based bioplastic inspired by nacre, to attain enhanced properties and effective

Table 7 EMIS performance of rPET composite materials by sonication and dip-coating

No.	Composite materials	Thickness (mm)	EMI SE (dB)	Frequency range (GHz)	References
1	rPET/FeCo@C/Ag90	0.103	68	8.2–12.4	109
2	rPET/FeCo@C/Ag90/PDMS20	0.103	68	8.2–12.4	109
3	rPET/Ag30	0.103	27	8.2–12.4	110
4	rPET/FeCo@C/Ag30	0.103	43	8.2–12.4	111
5	rPET/FeCo@C/Ag60	0.103	61	8.2–12.4	112

electromagnetic shielding. The bioplastic, referred to as SBP_{SCGM15}, was produced by self-assembling TEMPO-CNF modified starch, nano montmorillonite (NMMT), and reduced graphene oxide (rGO), resulting in a nacre-like layered structure.

Different starch-based bioplastic samples were named $SBPS_{CGMX}$, where S, C, G, and M represented the added starch, TEMPO-CNF, rGO, and NMMT, respectively, and *x* represented the proportion of NMMT added to the percentage of starch content. This distinctive configuration and strong interfacial interactions led to impressive mechanical features, including a tensile strength of 37.39 MPa. The bioplastic also exhibited improved water and heat resistance and a notable SE_T of 35 dB at a thickness of 0.5 mm. Moreover, SBP_{SCGM15} is characterized by its repairability, renewability, and biodegradability.[117] The nacre-inspired design of this starch-based bioplastic holds considerable potential for use in electromagnetic shielding applications. The vector network analyzer assessed the EMI SE of the SBP samples (30×20 mm^2), and the results are displayed in Table 8.[14]

FeCo/PANI composites. Polyaniline (PANI) is a conductive polymer with low density, unique dielectric characteristics, and environmental stability. It can be manipulated by doping agents, offering new opportunities for developing PANI with specialized functionalities. Xingyu Si *et al.*[118] achieved dual functionalities of hydrophobicity and excellent microwave transmission in a single material. A new template-free method for synthesizing PANI particles with bioinspired nanostructures was developed using camphor sulfonic acid. The unique structure of PANI imparts superior hydrophobicity and microwave transmission capabilities, which makes it ideal for applications in industries like telecommunications, aerospace, *etc.*

Electrically and magnetically hybrid nanocomposites have been created for a number of uses, such as energy generation, tissue engineering, sensors, microwave absorption and shielding, and storage. Potential biomedical uses for these materials include drug delivery systems, biosensors, and antibacterial materials. Ali Sedighi *et al.*[119] created iron oxide nanoparticles on polyester fabric using a two-step process, and poly-3,4-ethylenedioxythiophene (PEDOT) was added to the treated fabric to create a flexible textile-based conductive substrate with multiple uses. After iron oxide nanoparticles were added to the fabric, an electrically conductive PEDOT/iron oxide/PET fabric with an electrical resistivity of 1000 Ω cm^{-1} was produced. Incorporating nanoparticles improved PET fabric's tensile strength and strain, and PEDOT nanoparticles enhanced polyester or PET fabric's UV protection in UV B and UV C regions. This work creates the opportunity to make textiles with electrical and magnetic properties for wearable, flexible, and stretchable electronics.

D. Liu *et al.* examined the environmental challenges posed by secondary electromagnetic pollution resulting from reflections off metallic shields, underscoring the necessity for electromagnetic or microwave absorbing materials (MAMs) that can effectively absorb EM radiation and inhibit its further propagation.[120] According to P. Saini *et al.*, efficient electromagnetic absorbing materials incorporate lossy media featuring electric/magnetic dipoles and mobile charge carriers that engage with incoming radiation, converting energy into heat.[27] These materials are expected to possess advantageous characteristics, including low weight, corrosion resistance, and a wide absorption coefficient across various frequencies. Intrinsically conducting polymers such as polyaniline, polypyrrole, and polythiophene are noted for their commendable dielectric properties, adjustable conductivity, and flexibility.[121] Moditma *et al.*[122] highlighted the EMIS performance of uniformly dispersed FeCo/polyaniline composites created through a simple grind-mixing approach. Initial tests utilized the non-conducting form of polyaniline (emeraldine base, EB) to evaluate how magnetic FeCo nanoparticles enhance absorption capabilities.

Further investigations concentrated on composites made with the conducting form of polyaniline (emeraldine salt, ES), which exhibited marked improvements in SE. The grind mixing technique was used to create a composite of FeCo nanoparticles in emeraldine bases (PANI-EB) and emeraldine salt (PANI-ES) forms of polyaniline.[123] The uniform distribution of the FeCo nanoparticles was achieved by FE-SEM imaging and elemental mapping. The structural and magnetic characteristics of the implanted alloy were unchanged throughout the physical mixing operation. While emeraldine base composites had weak EMIS characteristics, composites containing the emeraldine salt form of polyaniline showed excellent electromagnetic (EM) wave absorbing capabilities in the X band, with an overall shielding efficacy of 40 dB at 25 wt% FeCo filling. This was largely related to the basic polymer's outstanding dielectric characteristics, which were greatly improved upon FeCo addition, and the contribution of magnetic and conduction losses caused by these nanoparticles. Thus, the generated magnetic composites had superior impedance-matching properties, resulting in lower losses owing to reflection and absorption-dominated shielding. Table 9 shows the EMIS capability of SBP samples.

Further development of shielding capabilities is predicted by appropriate linkage with nano-carbon derivatives/magnetic iron oxides in these samples in order to boost shielding efficiency

Table 8 EMIS performance of SBP samples (30×20 mm^2) by the self-assembly method

No.	Composite materials	Thickness (mm)	EMI SE (dB)	Frequency range (GHz)	References
1	SBP_{SCGM15}	0.5	35.95	8.2–12.4	14
2	SBP_{SGM}	0.5	28.45	8.2–12.4	14

Table 9 EMIS performance of SBP samples (30 × 20 mm^2) by the grind mixing technique

No.	Composite materials	Thickness (mm)	EMI SE (dB)	Frequency range (GHz)	References
1	PANI-ES/FeCo (25 wt%)	1.5	40	8.2–12.4	122
2	PANI-ES/FeCo/graphene	1.5	53	8.2–12.4	122

without significantly affecting the light-weight sample quality.[124–126]

Template-free synthesis of PANI nanostructures. According to recent studies, appropriate structures can greatly customize EMIS capabilities. Vertically growing hierarchical columnar ZnO arrays on carbon cloth, for instance, can reach a minimum SE_R value of −39.6 dB at a thickness of 3.5 mm (ref. 127) and porous structures can raise the minimum SE_R value to −48.1 dB at a thickness of 3.5 mm.[128] The benefits of intrinsically conductive polymers (ICPs) include their low density, tunable dielectric behaviours, and ease of synthesis. The distinctive doping mechanism of PANI, which enables adjustable dielectric properties over a broad frequency range, makes it a promising candidate for EMIS applications.[129]

PANI particles with the desired structures are created in order to solve this issue, and they demonstrate efficient EMIS properties. In order to create PANI-based composites with a helical structure and improve polarisation characteristics, dielectric loss, and microwave attenuation properties, spiral-structured cotton fiber is used as a template.[130] Using the steric stabiliser polyvinyl pyrrolidone (PVP) as a template, PANI particles are created using the reverse dropping technique.[131] Although the template approach provides more flexibility, it may weaken the overall dielectric network of PANI, which would lower its absorption capacity.

According to J. Yang *et al.*,[132] the chemical makeup of PANI, which is mostly dictated by the oxidation state and doping rate, is intimately linked to its dielectric properties. This study presents a simple and effective template-free technique for creating PANI particles with delicate nanostructures, such as nanosheets, clusters, and nanofibers. With a maximum Effective Absorption Bandwidth (EAB) of 6.12 GHz and a minimum SE_R value of −52.22 dB at 9.84 GHz, the obtained PANI shows outstanding EMIS performance. These PANI particles are crucial for applications in a number of industries, including communications, defence, aerospace, and precision electronics, due to their potent absorption capacity.

The EMIS efficiency of different PANI-based composites is given in Table 10.

Flexible nickel chains/acrylate composites. Pressure-sensitive adhesives (PSAs) promise rapid bonding under minimal pressure that can be maintained by repeated adhesion.[135] Nickel (Ni) particles, with their high aspect ratio and anisotropy, are an excellent functional filler for providing EMI shielding qualities to PSAs.[136] H. Zhang *et al.* proposed a simple and versatile approach for creating functional adhesives with very effective and customizable EMI shielding capability.[137]

A method for creating EMI shielding functional adhesives that is simple, practical, scalable, and effective has been created by C. Wang *et al.*[138] The adhesive matrix is made of acrylate-based PSA (a-PSA), and the functional electromagnetic shielding adhesive is created by integrating Ni chains with a-PSA. The unique layered structure is critical in defining shielding efficiency and adhesive strength, which can be easily adjusted by varying the Ni chain concentration. The composite adhesives with different Ni chains/a-PSA mass ratios of 1 : 9, 2 : 8, 2.5 : 7.5, 3 : 7, 3.5 : 6.5, 4 : 6, and 5 : 5 were fabricated through repeated solution casting processes. PSA-3 showed a maximum EMIS of 39.97 dB with a small thickness of 0.18 mm, while preserving high bonding performance.

Other PSA methods can readily replace the suggested electromagnetic adhesive prototype to produce electromagnetic shielding adhesives. Both a-PSA and Ni chains are commercially accessible and reasonably priced, and the production and application processes are simple and effective. Because of these characteristics, the functional adhesive has excellent potential for use in wearable smart devices and sophisticated flexible electronics. The adhesive properties and EMI shielding performance are significantly influenced by the spatial distribution of Ni chains. With just a gentle finger touch, the composite adhesive can be effortlessly affixed to a variety of material surfaces.

Y. Zhang *et al.*[139] successfully synthesised a hierarchical BF/PANI composite with a core–shell structure in a one-step *in situ*

Table 10 EMIS of PANI-based materials

No.	Composite materials	Processing method	Thickness (mm)	EMI SE_R (dB)	Frequency range (GHz)	References
1	PANI	Chemical oxidation polymerization	3.2	−52.12	6.12	132
2	Fe_3O_4@PANI	Hydrothermal	1.6	−55.50	17.3	133
3	Sepiolite/La-barium ferrite@PANI	*In situ* chemical oxidation	2.4	−71.98	2–18	134

polymerisation of polyaniline (PANI) on bagasse fibre (BF). The composite exhibits a superior EMIS of 28.8 dB with a thickness of only 0.4 mm, mainly due to increased electrical conductivity and effective multiple reflections. This versatile and cost-effective method is expected to enable efficient utilisation of low-cost natural materials in EMI shielding applications.

Carbon–polymer based nanocomposites

Hybrid CNT and CF reinforced PEEK composites. Various fabrication methods, including melt blending[140,141] and solution compounding,[141,142] are commonly employed for CNT-based polymer nanocomposites, but issues such as the use of toxic solvents, increased viscosity with high CNT loading, filler breakage, and polymer degradation can occur if process parameters are not carefully controlled.[143] While techniques like chemical vapor deposition,[144] electrophoretic deposition,[145,146] and *in situ* polymerization[147] can address some of these limitations, they present challenges for large-scale production. Recently, spray coating has emerged as a cost-effective and scalable method for incorporating CNTs into polymer composites. For instance, S. Cao *et al.*[7] developed multi-walled carbon nanotube (MWCNT)/carbon fiber (CF)/polyether ether ketone (PEEK) composites with a multi-layer structure, which were fabricated using spray coating to deposit CNTs on each layer, and their effects on morphology, mechanical properties, interlaminar bonding, and EMIS were investigated. Unlike earlier studies that focused on the mechanical and electrical properties of CF/PEEK composites or the EMI properties of other polymers, this research addressed high-temperature applications such as aerospace and offshore telecommunications, which require materials capable of withstanding temperatures up to 250 °C. The optimal CNT content of 1.5 g m^{-2} (0.32 wt%) resulted in a uniform conductive network, improving tensile and flexural strength and enhancing interlaminar bonding, as shown by dynamic mechanical analysis (DMA).

The resistance of CF/MWCNT/PEEK laminates with varying interlaminar MWCNT content (0.0 g m^{-2}, 0.5 g m^{-2}, 1.5 g m^{-2}, 2.5 g m^{-2}, 4.5 g m^{-2}) was evaluated in the plane direction using a B2912a (Keysight) source meter and silver paint applied to the sample edge along the width. The conductivity may be computed as

$$\sigma = \frac{L}{RS} \tag{12}$$

where the sample resistance (R), cross-sectional area (S), and length perpendicular to the current flow (L) are used in resistance measurement. Table 11 displays the electrical conductivity of MWCNT/CF/PEEK composites based on MWCNT loading in g m^{-2} and weight percentage.

The CNTs were more effective in improving flexural properties due to their ability to strengthen the inter-ply region under bending forces. However, excessive CNT content led to cluster formation, diminishing mechanical properties. The highest EMI SE of 43.2 dB was achieved at 2.5 g m^{-2} (0.53 wt% CNT), after which both conductivity and EMI performance declined. This study is the first to demonstrate the effectiveness of spray-coating CNTs in enhancing the EMI performance of carbon fiber-reinforced PEEK composites.

The EMIS sample size is 22.9 mm × 10.2 mm × 1.7 mm. The SE_T of carbon@polyaniline nanorod array microspheres (C@PANI), novel CF@$NiFe_2O_4$ composite coated with phytic acid-doped polyaniline (CF@$NiFe_2O_4$@p-PANI), MWCNT, *etc.* is shown in Table 12.

Hybrid epoxy composites. The growing demand for carbon fiber reinforced polymer composites (CFRPs) in the aviation sector, primarily for their fuel-saving benefits, despite their limited EMIS capabilities. Epoxy (EP) is a widely used thermosetting polymer, valued for its insulating qualities, dielectric behavior, strong adhesion, dimensional stability, chemical resistance, and rigidity.[157,158] While EP does not directly contribute to EMIS, it enhances filler connectivity, thus boosting overall shielding efficiency.[159] Carbon fibers (CFs) stand out due to their excellent strength-to-weight ratio, corrosion resistance, electrical conductivity, rigidity, low thermal expansion, and EMIS effectiveness.[160] Additionally, conductive polymers such as PPy and PANI are recognized for their potential in EMIS.[161,162] PPy-coated CFs improve interfacial adhesion with EP, creating high-performance composites.[163,164] Lastly, magnetite (Fe_3O_4) nanoparticles are noted for their size-dependent magnetic properties, transitioning from ferrimagnetic to superparamagnetic at smaller sizes. Larger particles (over 10 nm) enhance EMIS due to high magnetic permeability and dielectric properties,[165,166] while their hydrophilic nature strengthens interfacial bonding with EP resin.[167,168] Together, these materials pave the way for developing advanced CFRPs with enhanced EMIS, mechanical, and thermal characteristics.

R. Kanwal *et al.*[13] aimed to improve the mechanical properties and EMIS performance of hybrid composites made from PPy-coated CFs, magnetite nanoparticles (MP), graphene oxide (GO), and epoxy resin. PPy was coated onto desized carbon fiber

Table 11 Electrical conductivity of MWCNT/CF/PEEK composites[7]

No.	Interlaminar MWCNT loading (g m^{-2})	Total mass fraction (wt%)	Electrical conductivity (S cm^{-1})
1	0.0	0	6.46
2	0.5	0.11	8.35
3	1.5	0.32	8.90
4	2.5	0.53	10.87
5	4.5	0.96	10.45

Table 12 EMI SE comparison of nanofiller-reinforced polymer composites

No.	Filler/matrix	Processing method	Sample thickness (mm)	Mass fraction (wt%)	EMI SE (dB)	Frequency range (GHz)	References
1	CF/MWCNT	Spray-hot pressing	1.7	0.53	43.2	8.2–12.4	7
2	MWCNT	Melt blending	2.0	12	55	8.2–12.4	141
3	$BaTiO_3$	Melt blending	2.0	18	11	8.2–12.4	148
4	MWCNT	Melt extrusion	0.18	9	10.5	8.2–12.4	140
5	MWCNT/Fe_3O_4	Melt extrusion	0.50	9/4	27.2	8.2–12.4	141
6	Ni-CF	Electroplating melt extrusion	0.6	40	29	8.2–12.4	150
7	GNP/CLF	Compression moulding	2.5	2.5/9	27.1	8.2–12.4	12
8	CNF (or CNT)	Ultrasonic dispersion spraying	1.0	20 (or 5)	19.8 (24.1)	8.2–12.4	151
9	CNT/CF	Dry spray deposition	0.5	2.5 (g m^{-2})	53	8.2–12.4	152
10	MWCNT/CF	Sonication mechanical mixing method	0.5	1/50	60	8.2–12.4	153
11	C@PANI	Dilute polymerization	2.2	—	−59.60	15.5	154
12	CF@$NiFe_2O_4$@p-PANI	*In situ*	2.5	—	−64	5	155
13	MWCNT/CF	Chemical vapor deposition	2	3/27 (vol%)	51.1	8.2–12.4	156

mats using electrophoretic deposition, while GO and MP were produced using modified versions of Hummers' and Massart methods. The hybrid composites were fabricated *via* a vacuum bagging process to create porosity-free structures, with nanofillers added to the epoxy matrix through solution mixing and vacuum processing.

DC conductivity was determined using the two-probe method, which involved measuring resistance R using two multimeter probes. A 10 × 30 mm specimen was utilized for measurement. DC conductivity was measured using the following formulae.[13]

$$\text{DC Resistivity, } \rho = \frac{RA}{L} \tag{13}$$

$$\text{DC Conductivity, } \sigma = \frac{1}{\rho} \tag{14}$$

where R is the resistance in Ω, A is area in m^2, and L is the sample length in m.

Mechanical properties were assessed through tensile testing, and EMIS was evaluated in the X-band frequency range. Composites with 0.2 wt% GO demonstrated superior mechanical properties compared to those with higher GO content (0.8 wt%), and increased nanofiller content also improved DC conductivity.

The hybrid composite containing 0.2 wt% GO and 0.2 wt% MP exhibited the best combination of mechanical strength and EMIS due to effective impedance matching and electromagnetic wave attenuation. These composites show potential for use in structural materials, electronics packaging, and aerospace industries due to their enhanced mechanical and EMIS capabilities. The SE_T of different composite materials is shown in Table 13, which includes a ternary hybrid nanocomposite comprising thermoplastic polyurethane as the matrix and graphene nanoplatelets–carbon nanotube hybrid (GCNT) as filled inclusion. Also, the preparation method and SE values of $Fe_4[Fe(CN)_6]_3$ (Prussian blue), graphene oxide (GO) and magnetite (Fe_3O_4) nanocomposite is shown in the table. In another study, ordered mesoporous carbon (OMC)/fused silica composites with different carbon contents have been prepared by a controllable but simple sol–gel method followed by hot-pressing.

Activated carbon-embedded copper oxide nanoparticles/epoxy hybrid composites. The development of lightweight EMIS epoxy-based composites with high mechanical strength is very important for aircraft applications.[173] It emphasizes the increasing adoption of carbon fibre–reinforced polymer composites (CFRPs) in both commercial and military aircraft, replacing materials like aluminium and titanium alloys due to their excellent mechanical strength, corrosion resistance, and lightweight nature, which contribute to lower fuel consumption.[174,175]

However, CFRPs fall short in providing effective EMIS compared to aluminium, sparking research efforts to improve their SE. Various studies have explored incorporating conductive and magnetic fillers into CFRPs to enhance shielding performance. For example, the inclusion of multiwalled carbon nanotubes in carbon fibre-reinforced epoxy composites resulted in an SE of −60 dB,[153] while nickel and cobalt-coated biocarbon nanofiber/paraffin wax composites achieved an SE of 41.2 dB.[176]

K. S. Anu *et al.*[173] developed lightweight copper oxide-activated carbon (CuO-AC) nanoparticle-based epoxy composites for EMIS, filling a critical gap in studies on CuO-based composites. The study examines different weight ratios of CuO-AC nanoparticles, produced *via* a co-precipitation method, and their integration into an epoxy matrix to enhance mechanical strength and EMIS effectiveness.[173] The composite containing 10 wt% CuO-AC exhibited optimal mechanical performance and an SE of −36.33 dB at 11.44 GHz. To further boost performance, the composite was reinforced with 2-ply plain woven carbon fiber, leading to significant improvements in both EMIS of −52.02 dB and mechanical properties, driven by the combined effects of ohmic and dielectric losses.

Al-Ghamdi *et al.*[177] fabricated a novel functional nano conducting composite from polyvinyl chloride reinforced graphite–copper nanoparticles (PVC/GCu). A higher GCu loading level

Table 13 EMI SE of hybrid epoxy composite materials

No.	Composite materials	Processing method	Sample thickness (mm)	EMI SE_T (dB)	Frequency range (GHz)	References
1	0.2% GO–0.2% MP-CFPPy	Vacuum infusion	—	46.72	8.2–12.4	13
2	PVDF/FLG–3 wt% NSF–15 wt% hybrid polymer	Solution processing	1.2	53	8.2–12.4	169
3	10 wt% GCNT polyurethane	Solution blending	—	−47	12.4–18	170
4	$Fe_4[Fe(CN)_6]_3$/GO/Fe_3O_4 (PBGF)	Hummer's method	—	−51.66	8.2–12.4	171
5	10 vol% CNT/fused silica	Sol–gel	—	30	8.2–12.4	172
6	10 vol% OMC/fused silica	Sol–gel	—	40	8.2–12.4	172

has greater EMI SE shielding effectiveness reaching 70 dB in the frequency range of 1–20 GHz. Priyanka Rani *et al.*[178] prepared montmorillonite (MMT) nanoclay and copper oxide (CuO) nanoparticle (NP) reinforced polyvinylchloride (PVC)-based flexible nanocomposite films *via* the solvent casting technique having an SE_A of −30 dB in the X-band and −35 dB in the Ku-band.

These results indicate that the carbon fiber–reinforced CuO-AC/epoxy hybrid composite, with its enhanced thermal, mechanical, and EMIS properties, is highly suitable for aircraft applications, particularly within the X-band frequency range (8–12 GHz), critical for air traffic control and weather monitoring. EMIS epoxy hybrid composite materials for aircraft applications are shown in Table 14.[179]

Recycled carbon fiber–reinforced composites. The main techniques for extracting carbon fibers (CFs) from resin matrices include thermal decomposition and chemical degradation,[180–182] both of which are affected by polymer chemical bonds and crosslinking density, resulting in limited recycling efficiency and unpredictable decomposition for multi-component polymers.[183] In contrast, pyrolysis is regarded as the most cost-effective and sustainable method for industrial carbon fiber recycling due to its efficiency in terms of resources and processes.[184,185] To improve the interfacial adhesion between recycled carbon fibers (rCFs) and resin matrices, surface modification techniques have been developed, with dopamine (DA) being particularly effective. DA forms covalent bonds in the presence of oxygen and significantly enhances the adhesion and overall performance of rCF-reinforced composites, which are suitable for various applications.

K. Wang *et al.*[183] presented a detailed recycling strategy for addressing the conductivity degradation of recycled carbon fibres (rCFs) while increasing their use in rCF-reinforced composites. The method combines controllable pyrolysis and surface modification techniques, using a two-step pyrolysis procedure to decompose a phenolic resin matrix and eliminate carbon remnants from the fibre surfaces by varying the heat conditions during treatment. Following pyrolysis, polydopamine (pDA) is used to change the surface properties of the fibres, allowing chemical bonding with the phenolic resin and producing composites with excellent EMIS and flame retardant properties. A schematic diagram of recycling rCFFs and reassembling composites and SEM image is shown in Fig. 5.[186]

The study investigates the structural evolution and microstructure–property relationships of the rCFs to refine the pyrolysis parameters, showing consistent EMIS performance

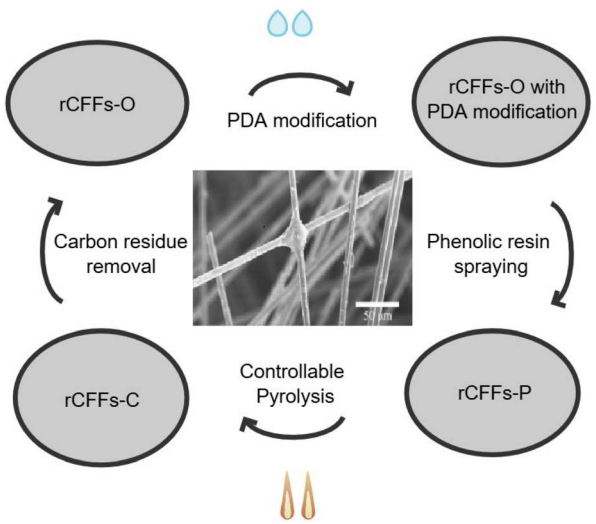

Fig. 5 The synthesis schematic diagram of the recycling and the reconstruction of the rCFF-based materials; the SEM image of rCFFs.[149]

Table 14 EMIS effectiveness of epoxy hybrid composite materials

No.	Composite materials	Processing method	Sample thickness (mm)	EMI SE (dB)	Frequency range (GHz)	References
1	CF–reinforced CuO-AC/epoxy hybrid composite	Co-precipitation	—	−52.02	11.48	173
2	PVC/GCu	In situ	2	70	1–20	177
3	PVC/MMT/CuO	Solvent casting	—	−30	8–12	178

Table 15 EMIS effectiveness of rCFF-based materials by a two-step pyrolysis method

No.	Composite materials	Processing method	Sample thickness (mm)	EMI SE (dB)	Frequency range (GHz)	References
1	rCFFs	Pyrolysis	0.3	30	8.2–12.4	185
2	rCFFs-P	Phenolic resin spraying	0.3	40.56	8.2–12.4	187
3	rCFFs-C	Two-step pyrolysis	0.3	47.72	8.2–12.4	188
4	rCFFs-O	Oxidation	0.3	36.95	8.2–12.4	189
5	4-layered rCFFs-O	Pyrolysis	1.2	70.50	8.2–12.4	183
6	rCFFs-C1	Pyrolysis	0.3	41.71	8.2–12.4	190
7	rCFFs-O1	Pyrolysis	0.3	36.90	8.2–12.4	191
8	rCFFs-O3	3rd pyrolysis	0.3	40.80	8.2–12.4	192

even after ten recycling cycles. The rCF-reinforced composites achieve an average SE_T of 40.56 dB in the X-band, potentially enhancing this to 70.50 dB through structural modifications.

Moreover, the modified rCFs demonstrate stable EMIS performance of 30.64 dB after multiple recycling cycles.[183] This approach not only offers an effective solution for recycling carbon fibers from waste composites but also establishes a method for surface modification that improves the performance of rCF-based materials, thereby supporting sustainable practices within the circular economy. The total EMI SE (SE_T) values in the X band of the rCFF-based materials are shown in Table 15.

Carbon fiber reinforced phenolic resin-based carbon composite foam. Zhao *et al.* reported the development of a composite based on MXene, achieving SE_T values of 25 dB in the X-band (8.2–12.4 GHz) and 30 dB in the Ku-band (12.4–18 GHz).[193] Similarly, Hu *et al.*[194] created delaminated MXene decorated with nickel (Ni) particles, yielding a minimal reflection loss of −50.36 dB. Agarwal *et al.*[195] produced carbon foam reinforced with manganese dioxide (MnO_2), demonstrating a specific EMI SE of 150 dB cm^3 g^{-1} within the 8.2–12.4 GHz frequency range.

Muzaffar *et al.*[196] formulated a polyvinyl chloride composite reinforced with nickel oxide (NiO) and tungsten oxide (WO_3), achieving an EMI SE of 15.8 dB in the X-band. More recently, Song *et al.*[197] presented zinc oxide (ZnO) nanoparticle-modified mesoporous carbon spheres, which displayed an EMI SE of 39.3 dB at 10.4 GHz. Additionally, Song *et al.*[198] developed multifunctional silicon carbide (SiC) aerogels reinforced with nanofibers and nanowires, achieving a minimum reflection loss (RL) of −61.56 dB, indicating their effectiveness for thermal energy regulation applications.[199]

V. K. Patle *et al.*[200] investigated the use of nickel (Ni) and iron (Fe) nanoparticles on carbon fibers, which were then integrated into carbon foam. The foam was fabricated using a sacrificial template method and carbonized at 1000 °C. The resulting composite foam featured carbon fibres decorated with Ni and Fe nanoparticles, resulting in a uniform distribution of Ni@C and Fe@C throughout the carbon matrix.[200]

Keju Ji *et al.*[201] prepared Cu–Ni open-cell foams with different pore densities by electrodeposition of Ni on a copper foam substrate. Zhimin Fan *et al.*[202] fabricated a lightweight MXene/graphene hybrid foam (MX–rGO) by freeze-drying and reduction heat treatment. H. G. Shi *et al.*[203] prepared a hybrid foam by using a 3D melamine-formaldehyde (MF) foam skeleton, 0D ferroferric oxide (Fe_3O_4) nanoparticles, and 1D silver nanowires (AgNWs) *via* coprecipitation and dip-coating processes. A comparison of these recently reported porous carbon materials with different additives and their corresponding EMIS performance is shown in Table 16.[200]

The carbon fibres displayed an SE_T of 24.5 dB, which was improved to a peak of 62.3 dB at 8.2 GHz for the Fe@C-CF composite. The Ni@C-CF and Fe@C-CF composite foams displayed absorption-dominant EMIS characteristics with minimal reflection components.[11] Additionally, these composite foams exhibited notable mechanical strength, making them promising candidates for lightweight EMIS shielding materials designed for high-performance electromagnetic wave absorption applications.[200]

Table 16 EMI SE of porous carbon materials with different additives in the 8.2–12.4 GHz frequency range

No.	Materials	Processing method	Density (g cm^{-3})	Thickness (mm)	EMI SE (dB)	References
1	Fe@C-CF	Sacrificial template	0.36	2.5	62.3	200
2	Cu–Ni alloy-CNT foam	Electro deposition	0.23	1.5	54.6	201
3	Carbon foam with Ni–Zn ferrite	Sol–gel & foaming	1.72	3.0	42	204
4	Carbon foam with Ag particles	Powder molding	0.58	4.0	33	205
5	MX–rGO hybrid foam	Freeze-drying and heat	0.0037	0.3	50.7	202
6	AgNWs/Fe_3O_4/MF foam	Coprecipitation and dip-coating	0.022	5.0	49.0	203
7	MXene/PCF foam	Steam foaming & carbonization	0.35	3.0	74	206

Comparison of various fabrication methods

Among the three categories mentioned, the polymer-based composites stand out in terms of maximum EMI shielding performance. Using a basic *in situ* polymerisation technique, Gao *et al.*[94] produced a 3D porous Ni/PANI composite foam with remarkable shielding efficiency ranging up to 93.8 dB. The synergistic effects of the 3D porous heterostructure enable many reflections, strong interfacial polarisation, and effective electromagnetic wave absorption. All of these effects together help to explain this remarkable shielding capability. The great shielding ability of this polymer-based composite emphasizes its possibilities for uses demanding strong EMI protection.

Real-world applicability depends critically on the mechanical flexibility, durability, and environmental stability of the EMIS composites in addition to high shielding performance and scalability. Chen *et al.*[5] prepared a flexible, multilayer CSNA composite film that shows excellent mechanical characteristics and a significant shielding of 38.6 dB even under 100% strain. Retaining 99.0% of its original value even after 10 000 times of bending, the flexible polyethylene terephthalate/polyaniline (PET/PANI) composite paper reported by Zhang *et al.*[32] also showed outstanding bending durability and shielding stability. These results highlight the need for creating strong mechanical and environmental performance EMIS materials to satisfy the needs of wearable devices, flexible electronics, and other useful applications.

The *in situ* polymerization method is the most promising of the three categories when it comes to scalable and economical composite preparation methods. Gao *et al.*[94] reported an *in situ* polymerisation method for producing the Ni/PANI foam again, which is one of the easy, effective, and eco-friendly procedures that is readily scalable for large-scale manufacturing on the basis of the comparison study. Similar to this, the spray coating technique by Cao *et al.*[7] for creating the MWCNT/CF/PEEK multilayer composites provides a scalable and economical means of adding conductive fillers to polymer matrices. These methods are appealing for the large-scale production of EMIS materials since they do not require the use of potentially dangerous solvents, complex equipment, or energy-intensive processing.

On comparing different fabrication methods, the spray coating and *in situ* polymerisation processes have obvious scalability and economic viability for mass production in the automotive or electronics sectors.[32,94] These techniques have advantages for the industrial-scale production of EMIS materials since they do not require the use of toxic solvents, sophisticated equipment, or energy-intensive processes. Furthermore, the internal and exterior reflections contribute to the remarkable shielding capabilities of polymer-based composites, especially PET/PANI composite paper and Ni/PANI foam.

The structural integrity, homogeneity, and EMI performance of the composites can be much influenced by the fabrication method chosen. Strong interfacial polarisation and a well-defined 3D porous heterostructure produced by Gao *et al.*[94] from their *in situ* polymerization method supported to explain the remarkable shielding effectiveness. The spray coating technique by Cao *et al.*,[7] on the other hand, needed careful control of the CNT deposition to obtain a homogeneous conductive network and improve the mechanical and EMI shielding characteristics. Chen *et al.*[5] used a magnetic alignment of the carbonyl iron@SiO_2 and Ni@Ag microparticles that allowed exact control of the composite structure and shielding mechanism, resulting in high shielding effectiveness. But, the complexity of the process could lead to difficulties for homogeneity and scalability. Overall, the *in situ* polymerization and spray coating techniques generally demonstrated superior EMI shielding performance, structural integrity, and homogeneity compared to other methods like solution casting or melt blending, which can be attributed to the enhanced absorption, reflection, and multiple reflection losses achieved through these fabrication approaches.

Drawbacks of the composites

The carbon-based materials, like carbon/graphite, can be fragile, while aluminium lacks impact resistance, and stainless steel is heavy and subject to corrosion, particularly in marine environments. These properties can limit the long-term durability and recyclability of carbon-based EMIS composites. From a sustainability perspective, carbon-based nanocomposites, including those incorporating carbon nanotubes (CNTs), graphene, and carbon black, have environmental and economic challenges. Additionally, the energy-intensive production processes and potential toxicity of some carbon nanomaterials, like carbon nanotubes, may raise environmental and health concerns.

Polymer-based nanocomposites, such as rPET as a potential sustainable solution, conventional petroleum-based polymers can have limited biodegradability and recyclability, leading to waste accumulation and environmental pollution. The use of toxic solvents and additives in the production of polymer-based EMIS composites may also raise sustainability concerns.

For carbon–polymer hybrid nanocomposites, the combination of carbon-based materials and polymers may raise challenges in terms of end-of-life management and recyclability, since the separation and recovery of individual components can be complex. The energy-intensive processing and potential toxicity of some nanomaterials used in these hybrids may also impact their overall sustainability. Considering all these factors emphasises the need for further research into sustainable and biodegradable materials for EMIS applications. Addressing these aspects, such as material selection, production methods, and end-of-life management, will be crucial for developing truly sustainable EMIS solutions.

Current developments

Significant progress in EMIS composites has focused on enhancing their performance for modern electronic applications. Researchers have made notable advancements in combining MXenes with polymers, creating lightweight and highly conductive materials that provide efficient shielding. Additionally, 3D graphene structures, hybrid nanocomposites

with carbon nanotubes and silver nanowires, and foam-based composites with conductive fillers are at the forefront. These innovations are tailored to improve EMI absorption while maintaining mechanical strength and flexibility, making them ideal for applications in flexible electronics, wearable devices, and 5G technologies.

Future developments

Further investigation into sustainable and biodegradable materials for EMIS, such as starch-based bioplastics and recycled polymers, is crucial for advancing eco-friendly solutions while maintaining high shielding performance. This includes the development of more efficient and environmentally friendly fabrication methods, including green reduction techniques and scalable processes such as spray coating, enhancement of recycling processes for carbon fiber composites to improve their EMIS properties over multiple cycles *etc.* The future developments will include the investigation of novel hybrid materials combining multiple components (*e.g.*, carbon-based materials, conductive polymers, and magnetic nanoparticles) to achieve synergistic effects in EMIS and the optimization of material structures, such as 3D architectures and gradient designs, to enhance both mechanical properties and EMIS effectiveness. Researchers are investigating multifunctional materials that combine EMIS with other desirable properties, such as flame retardancy, thermal management, or self-healing capabilities.

Conclusions

The review of carbon-based, polymer-based, and carbon–polymer hybrid nanocomposites for EMIS applications reveals significant advancements in material design and performance. Carbon-based materials, particularly CNTs and graphene, demonstrate excellent electrical conductivity and EMI absorption properties, making them suitable for lightweight shielding solutions. Polymer-based composites offer versatility and ease of processing, with conductive polymers and metal oxide-filled matrices showing promise for flexible EMIS applications. Carbon–polymer hybrid nanocomposites emerge as a practical approach, combining the strengths of both components to achieve superior EMIS effectiveness. These hybrids often exhibit improved mechanical properties and thermal stability, addressing multiple engineering challenges simultaneously.

Among the carbon-based nanocomposites, the CSNA film developed by Chen *et al.*[5] demonstrated an impressive shielding effectiveness of 64.5 dB at a thickness of 1.6 mm, prepared by the magnetic alignment of carbonyl iron@SiO_2 and Ni@Ag microparticles. Moving to polymer-based composites, the PVA/PSSA nanocomposite film with 25 wt% TiO_2 nanoparticles exhibited a shielding effectiveness of 12–13 dB in the X-band and Ku-band at a thickness of 0.07 mm, showcasing the potential of sustainable and recyclable materials. In the category of carbon–polymer hybrid nanocomposites, the CNF/MWCNT@Fe_3O_4/MXene asymmetric multilayer composite membrane developed by Zhou *et al.*[48] achieved a remarkable shielding effectiveness of 73.2 dB at a thickness of 0.18 mm, highlighting the synergistic effects of the hybrid design. Other notable examples include the rPET/FeCo@C/Ag_{90}/$PDMS_{20}$ membrane with 68 dB shielding at 0.103 mm thickness, the SBP_{SCGM15} starch-based bioplastic with 35.95 dB shielding at 0.5 mm, and the PANI-ES/FeCo composite with 40 dB shielding at 1.5 mm thickness. These materials demonstrate the progress in developing EMIS composites with high performance, ease of processing, and sustainability considerations.

In conclusion, the field of EMIS materials continues to evolve rapidly, driven by the growing need for effective electromagnetic protection in an increasingly connected world. The integration of advanced carbon and polymer nanocomposites offers promising solutions for addressing EMI challenges across various industries, paving the way for the next generation of electronic devices and communication systems.

Data availability

The data supporting this article have been included in the references section of the manuscript and have been cited accordingly in the text.

Author contributions

Hareesh M. S.: investigation, data curation, scientific discussion, writing – original draft. Praveen Joseph: investigation, data curation, scientific discussion, writing – original draft. Sumesh George: investigation, data curation, scientific discussion, writing – original draft, supervision. All authors contributed to writing – review editing and have given approval to the final version of the manuscript.

Conflicts of interest

There are no conflicts to declare that are relevant to the content of this article.

Acknowledgements

This research has received no external funding.

References

1 T.-T. Li, A.-P. Chen, P.-W. Hwang, Y.-J. Pan, W.-H. Hsing, C.-W. Lou, Y.-S. Chen and J.-H. Lin*, Synergistic effects of micro-/nano-fillers on conductive and electromagnetic shielding properties of polypropylene nanocomposites, *Mater. Manuf. Processes*, 2018, **33**, 149–155.

2 M. Gurusiddesh, B. J. Madhu and G. J. Shankaramurthy, Structural, dielectric, magnetic and electromagnetic interference shielding investigations of polyaniline decorated Co0.5Ni0.5Fe2O4 nanoferrites, *J. Mater. Sci.: Mater. Electron.*, 2018, **29**, 3502–3509.

3 P. Singh, V. K. Babbar, A. Razdan, S. L. Srivastava and T. C. Goel, Microwave absorption studies of Ca–NiTi hexaferrite composites in X-band, *Mater. Sci. Eng. B*, 2000, **78**, 70–74.

4 P. Saini, V. Choudhary, B. P. Singh, R. B. Mathur and S. K. Dhawan, Enhanced microwave absorption behavior of polyaniline-CNT/polystyrene blend in 12.4–18.0GHz range, *Synth. Met.*, 2011, **161**, 1522–1526.
5 T. Chen, J. Cai, D. Gong, X. Cheng, P. Liu and D. Zhang, Magnetically driven hierarchically ordered carbonyl iron@SiO2/Ni@Ag/silicone rubber composite film for enhanced electromagnetic interference shielding with ultralow reflection, *J. Mater. Chem. C*, 2023, **11**, 6597–6606.
6 M. E. Prince, K. Tamilarasi, S. M. K. Thiagamani, M. Hashem, H. Fouad and A. Z. Ansari, Effects of TiO2 nanoparticles on the dielectric and electromagnetic shielding performance of PVA/POM hybrid nanocomposites, *Polym.-Plast. Technol. Mater.*, 2024, **63**, 1874–1886.
7 S. Cao, Y. Tao, H. Li, M. Ren and J. Sun, Multiscale hybrid CNT and CF reinforced PEEK composites with enhanced EMI properties, *Nanocomposites*, 2022, **8**, 184–193.
8 F. Cao, J. Xu, X. Zhang, B. Li, X. Zhang, Q. Ouyang, X. Zhang and Y. Chen, Tuning Dielectric Loss of SiO2@CNTs for Electromagnetic Wave Absorption, *Nanomaterials*, 2021, **11**, 2636.
9 H. Liu, Y. Xu, H. Yong, Y. Huang, D. Han, K. Yang and Q. Yang, Studies on electromagnetic interference shielding effect mechanisms of leaf-like three-dimensional carbon nanotubes/graphene aerogel film and the composites with polydimethylsiloxane, *Carbon*, 2023, **207**, 261–269.
10 R. K. Mishra, J. Sarkar, K. Verma, I. Chianella, S. Goel and H. Y. Nezhad, Exploring transformative and multifunctional potential of MXenes in 2D materials for next-generation technology, *Open Ceram.*, 2024, **18**, 100596.
11 B. Kaidar, A. Imash, G. Smagulova, A. Keneshbekova, R. Kazhdanbekov, E. Yensep, D. Akalim and A. Lesbayev, Magnetite-Incorporated 1D Carbon Nanostructure Hybrids for Electromagnetic Interference Shielding, *Nanomaterials*, 2024, **14**, 1291.
12 S. Li, W. Li, J. Nie, D. Liu and G. Sui, Synergistic effect of graphene nanoplate and carbonized loofah fiber on the electromagnetic shielding effectiveness of PEEK-based composites, *Carbon*, 2019, **143**, 154–161.
13 R. Kanwal, M. F. Maqsood, M. A. Raza, A. Inam, M. Waris, Z. U. Rehman, S. M. Z. Mehdi, N. Abbas and N. Lee, Polypyrrole coated carbon fiber/magnetite/graphene oxide reinforced hybrid epoxy composites for high strength and electromagnetic interference shielding, *Mater. Today Commun.*, 2024, **38**, 107684.
14 D. Xie, R. Zhang, S. Song, S. Yang, A. Yang, C. Zhang and Y. Song, Nacre-inspired starch-based bioplastic with excellent mechanical strength and electromagnetic interference shielding, *Carbohydr. Polym.*, 2024, **331**, 121888.
15 S. K. Dhawan, A. Ohlan and K. Singh, Designing of Nano Composites of Conducting Polymers for EMI Shielding, *Adv. Nanocompos. Synth.: Synth., Charact. Ind. Appl.*, 2011, DOI: **10.5772/14752**.
16 D. Jiang, V. Murugadoss, Y. Wang, J. Lin, T. Ding, Z. Wang, Q. Shao, C. Wang, H. Liu, N. Lu, R. Wei, A. Subramania and Z. Guo, Electromagnetic Interference Shielding Polymers and Nanocomposites - A Review, *Polym. Rev.*, 2019, **59**, 280–337.
17 J. T. Orasugh, C. Pal, M. S. Ali and D. Chattopadhyay, in *Polymer Nanocomposites Containing Graphene*, Elsevier, 2022, pp. 211–243.
18 Q. Xie, Z. Yan, F. Qin, L. Wang, L. Mei, Y. Zhang, Z. Wang, G. Zhao and R. Jiang, Metal carbide/Ni hybrids for high-performance electromagnetic absorption and absorption-based electromagnetic interference shielding, *Inorg. Chem. Front.*, 2020, **7**, 4832–4844.
19 H. W. Ott and H. W. Ott, *Noise Reduction Techniques in Electronic Systems*, Wiley, New York, 1988, vol. 442.
20 S. Geetha, K. K. Satheesh Kumar, C. R. K. Rao, M. Vijayan and D. C. Trivedi, EMI shielding: Methods and materials—A review, *J. Appl. Polym. Sci.*, 2009, **112**, 2073–2086.
21 S. Sankaran, K. Deshmukh, M. B. Ahamed and S. K. Khadheer Pasha, Recent advances in electromagnetic interference shielding properties of metal and carbon filler reinforced flexible polymer composites: A review, *Composites, Part A*, 2018, **114**, 49–71.
22 Dept. of Electronics & Communication Engineering, USICT, (GGSIPU), India, M. Rai and R. Kumar Yadav, Characterization of Shielding Effectiveness of General Metallized Structure, *Int. J. Wirel. Microw. Technol.*, 2014, **4**, 32–45.
23 L. Liang, G. Han, Y. Li, B. Zhao, B. Zhou, Y. Feng, J. Ma, Y. Wang, R. Zhang and C. Liu, Promising $Ti_3C_2T_x$ MXene/Ni Chain Hybrid with Excellent Electromagnetic Wave Absorption and Shielding Capacity, *ACS Appl. Mater. Interfaces*, 2019, **11**, 25399–25409.
24 D. D. L. Chung and M. Ozturk, Radio-wave absorption by aluminum and its dependence on the absorption distance, *J. Mater. Sci.*, 2021, **56**, 9263–9273.
25 P. Saini, V. Choudhary, B. P. Singh, R. B. Mathur and S. K. Dhawan, Polyaniline–MWCNT nanocomposites for microwave absorption and EMI shielding, *Mater. Chem. Phys.*, 2009, **113**, 919–926.
26 H. W. Ott and H. W. Ott, *Electromagnetic Compatibility Engineering*, Wiley, Hoboken, New Jersey, 2009.
27 P. Saini and M. Aror, Microwave Absorption and EMI Shielding Behavior of Nanocomposites Based on Intrinsically Conducting Polymers, Graphene and Carbon Nanotubes, *New Polym. Spec. Appl.*, 2012, DOI: **10.5772/48779**.
28 *New Polymers for Special Applications*, ed. A. De Souza Gomes, InTech, 2012.
29 S. Liu, J. Yang, Y. Yu, D. Liang, Y. Li, X. Si, S. Song, M. Meng, J. Zhang and Y. Zhang, Multifunctional flexible carbon fiber felt@nickel composite films with core–shell heterostructure: Exceptional Joule heating capability, thermal management, and electromagnetic interference shielding, *Chem. Eng. J.*, 2024, **494**, 153221.

30 Y. Zhang, Z. Yang, T. Pan, H. Gao, H. Guan, J. Xu and Z. Zhang, Construction of natural fiber/polyaniline core-shell heterostructures with tunable and excellent electromagnetic shielding capability via a facile secondary doping strategy, *Composites, Part A*, 2020, **137**, 105994.

31 H. Zhang, T. Liu, Z. Huang, J. Cheng, H. Wang, D. Zhang, X. Ba, G. Zheng, M. Yan and M. Cao, Engineering flexible and green electromagnetic interference shielding materials with high performance through modulating WS2 nanosheets on carbon fibers, *J. Materiomics*, 2022, **8**(2), 327–334, DOI: **10.1016/j.jmat.2021.09.003**.

32 Y. Zhang, T. Pan and Z. Yang, Flexible polyethylene terephthalate/polyaniline composite paper with bending durability and effective electromagnetic shielding performance, *Chem. Eng. J.*, 2020, **389**, 124433.

33 D. Kumar, A. Moharana and A. Kumar, Current trends in spinel based modified polymer composite materials for electromagnetic shielding, *Mater. Today Chem.*, 2020, **17**, 100346.

34 B. Yao, W. Hong, T. Chen, Z. Han, X. Xu, R. Hu, J. Hao, C. Li, H. Li, S. E. Perini, M. T. Lanagan, S. Zhang, Q. Wang and H. Wang, Highly Stretchable Polymer Composite with Strain-Enhanced Electromagnetic Interference Shielding Effectiveness, *Adv. Mater.*, 2020, **32**, 1907499.

35 V. Rathi and V. Panwar, Electromagnetic Interference Shielding Analysis of Conducting Composites in Near- and Far-Field Region, *IEEE Trans. Electromagn. Compat.*, 2018, **60**, 1795–1801.

36 J. Kruželák, A. Kvasničáková, K. Hložeková and I. Hudec, Progress in polymers and polymer composites used as efficient materials for EMI shielding, *Nanoscale Adv.*, 2021, **3**, 123–172.

37 H. H. Park, Electromagnetic Shielding Analysis of Planar Materials Using ASTM D4935 Standard Fixture, *IEEE Trans. Electromagn. Compat.*, 2022, **64**, 1767–1778.

38 M. K. Mohanapriya, K. Deshmukh, J. Kadlec, K. K. Sadasivuni, M. Faisal, N. A. Nambi Raj and S. K. K. Pasha, Dynamic mechanical analysis and broadband electromagnetic interference shielding characteristics of poly (vinyl alcohol)-poly (4-styrenesulfonic acid)-titanium dioxide nanoparticles based tertiary nanocomposites, *Polym.-Plast. Technol. Mater.*, 2020, **59**, 847–863.

39 A. Joshi, A. Bajaj, R. Singh, P. S. Alegaonkar, K. Balasubramanian and S. Datar, Graphene nanoribbon–PVA composite as EMI shielding material in the X band, *Nanotechnology*, 2013, **24**, 455705.

40 P. Rani and R. S. Malik, Electromagnetic interference shielding behavior of polypyrrole-impregnated poly(ether imide)/sulfonated poly(ether ether ketone) composites, *Mater. Chem. Phys.*, 2023, **307**, 128187.

41 P. Saini, Historical review of advanced materials for electromagnetic interference (EMI) shielding: Conjugated polymers, carbon nanotubes, graphene based composites, *Appl Phys.*, 2019, **57**, 338–351.

42 D. Gong, L. Sun, X. Li, W. Zhang, D. Zhang and J. Cai, Micro/Nanofabrication, Assembly, and Actuation Based on Microorganisms: Recent Advances and Perspectives, *Small Struct.*, 2023, **4**, 2200356.

43 Y. Li, J. Liu, S. Wang, L. Zhang and B. Shen, Self-templating graphene network composites by flame carbonization for excellent electromagnetic interference shielding, *Composites, Part B*, 2020, **182**, 107615.

44 J. Yang, X. Liao, G. Wang, J. Chen, F. Guo, W. Tang, W. Wang, Z. Yan and G. Li, Gradient structure design of lightweight and flexible silicone rubber nanocomposite foam for efficient electromagnetic interference shielding, *Chem. Eng. J.*, 2020, **390**, 124589.

45 H. Li, X. Ru, Y. Song, H. Wang, C. Yang, S. Zheng, L. Gong, X. Zhang, H. Duan, Z. Liu, Q. Zhang and Y. Chen, Flexible Sandwich-Structured Silicone Rubber/MXene/Fe3O4 Composites for Tunable Electromagnetic Interference Shielding, *Ind. Eng. Chem. Res.*, 2022, **61**, 11766–11776.

46 D. Gao, S. Guo, Y. Zhou, B. Lyu, X. Li, P. Zhao and J. Ma, Absorption-Dominant, Low-Reflection Multifunctional Electromagnetic Shielding Material Derived from Hydrolysate of Waste Leather Scraps, *ACS Appl. Mater. Interfaces*, 2022, **14**, 38077–38089.

47 Z. Xie, Y. Cai, Y. Zhan, Y. Meng, Y. Li, Q. Xie and H. Xia, Thermal insulating rubber foams embedded with segregated carbon nanotube networks for electromagnetic shielding applications, *Chem. Eng. J.*, 2022, **435**, 135118.

48 Y. Zhou, B. Xue, L. Zeng, L. Xie and Q. Zheng, Asymmetric multilayered cellulose nanofiber composite membranes with electrical-magnetic dual-gradient architectures towards excellent electromagnetic interference shielding performance, *Compos. Sci. Technol.*, 2024, **255**, DOI: **10.1016/j.compscitech.2024.110729**.

49 M. Cheng, W. Ren, H. Li, X. Liu, S. Bandaru, J. Zhang and X. Zhang, Multiscale collaborative coupling of wood-derived porous carbon modified by three-dimensional conductive magnetic networks for electromagnetic interference shielding, *Composites, Part B*, 2021, **224**, 109169.

50 Y. Zhang, H. Meng, F. Lyu, X. Fan, P. Liu, X. He, Y. Huang, B. Chen, Y. Yang and J. Wei, Temporal characteristics of agarwood formation in Aquilaria sinensis after applying whole-tree agarwood-inducing technique, *Chin. Herb. Med.*, 2023, **15**, 37–44.

51 G. Hu, C. Wu, Q. Wang, F. Dong and Y. Xiong, Ultrathin nanocomposite films with asymmetric gradient alternating multilayer structures exhibit superhigh electromagnetic interference shielding performances and robust mechanical properties, *Chem. Eng. J.*, 2022, **447**, 137537.

52 C. He, L. Zeng, B. Xue, X. Zhang, L. Yu, L. Xie and Q. Zheng, Electromagnetic interference shielding composite aerogels with asymmetric structures developed in aid of neural network, *Compos. Sci. Technol.*, 2024, **251**, 110579.

53 J. Xu, S. Tang, D. Liu, Z. Bai, X. Xie, X. Tian, W. Xu, W. Hou, X. Meng and N. Yang, Rational design of hollow Fe3O4 microspheres on Ti3C2Tx MXene nanosheets as highly-efficient and lightweight electromagnetic absorbers, *Ceram. Int.*, 2022, **48**, 2595–2604.

54 B. Zhou, Z. Zhang, Y. Li, G. Han, Y. Feng, B. Wang, D. Zhang, J. Ma and C. Liu, Flexible, Robust, and Multifunctional Electromagnetic Interference Shielding Film with Alternating Cellulose Nanofiber and MXene Layers, *ACS Appl. Mater. Interfaces*, 2020, **12**, 4895–4905.

55 T. Gu, D. Sun, X. Xie, X. Qi, J. Yang, C. Zhao, Y. Lei and Y. Wang, Highly thermally conductive, electrically insulated and flexible cellulose nanofiber-based composite films achieved via stereocomplex crystallites cross-linked graphene nanoplatelets, *Compos. Sci. Technol.*, 2022, **230**, 109757.

56 K. Xue, T. de Cola, D. S. L. Wei, A. Pérez-Neira, H. S. Hassanein, L. Kuang and S. Chatzinotas, Guest Editorial: Space Information Networks: Technological Challenges, Design Issues, and Solutions, *IEEE Network*, 2021, **35**, 16–18.

57 M. Ma, X. Liao, Q. Chu, S. Chen, Y. Shi, H. He and X. Wang, Construction of gradient conductivity cellulose nanofiber/MXene composites with efficient electromagnetic interference shielding and excellent mechanical properties, *Compos. Sci. Technol.*, 2022, **226**, 109540.

58 F. Zhang, P. Ren, Z. Guo, J. Wang, Z. Chen, Z. Zong, J. Hu, Y. Jin and F. Ren, Asymmetric multilayered MXene-AgNWs/cellulose nanofiber composite films with antibacterial properties for high-efficiency electromagnetic interference shielding, *J. Mater. Sci. Technol.*, 2022, **129**, 181–189.

59 B. Zhou, Q. Li, P. Xu, Y. Feng, J. Ma, C. Liu and C. Shen, An asymmetric sandwich structural cellulose-based film with self-supported MXene and AgNW layers for flexible electromagnetic interference shielding and thermal management, *Nanoscale*, 2021, **13**, 2378–2388.

60 G. Sang, C. Wang, Y. Zhao, G. He, Q. Zhang, M. Yang, S. Zhao, P. Xu, X. Xi and J. Yang, Ni@CNTs/Al2O3 Ceramic Composites with Interfacial Solder Strengthen the Segregated Network for High Toughness and Excellent Electromagnetic Interference Shielding, *ACS Appl. Mater. Interfaces*, 2022, **14**, 4443–4455.

61 X. Shu, S. Yan, B. Fang, Y. Song and Z. Zhao, A 3D multifunctional nitrogen-doped RGO-based aerogel with silver nanowires assisted self-supporting networks for enhanced electromagnetic wave absorption, *Chem. Eng. J.*, 2023, **451**, 138825.

62 H. Liu, Y. Xu, D. Han, J.-P. Cao, F. Zhao and Q. Yang, Leaf-structured Carbon Nanotubes/Graphene Aerogel and the Composites with Polydimethylsiloxane for Electromagnetic Interference Shielding, *Mater. Lett.*, 2022, **313**, 131751.

63 P. Zhang, L. Yin, X. Yang, J. Wang, M. Chi and J. Qiu, Cotton-derived 3D carbon fiber aerogel to in situ support Bi2O3 nanoparticles as a separation-free photocatalyst for antibiotic removal, *Carbon*, 2023, **201**, 110–119.

64 Z. Chen, C. Xu, C. Ma, W. Ren and H. Cheng, Lightweight and Flexible Graphene Foam Composites for High-Performance Electromagnetic Interference Shielding, *Adv. Mater.*, 2013, **25**, 1296–1300.

65 X. Sun, X. Liu, X. Shen, Y. Wu, Z. Wang and J.-K. Kim, Graphene foam/carbon nanotube/poly(dimethyl siloxane) composites for exceptional microwave shielding, *Composites, Part A*, 2016, **85**, 199–206.

66 Q. Gao, G. Zhang, Y. Zhang, X. Fan, Z. Wang, S. Zhang, R. Xiao, F. Huang, X. Shi and J. Qin, Absorption dominated high-performance electromagnetic interference shielding epoxy/functionalized reduced graphene oxide/Ni-chains microcellular foam with asymmetric conductive structure, *Compos. Sci. Technol.*, 2022, **223**, 109419.

67 M. Li, M. Zhang, Y. Zhao, S. Jiang, Q. Xu, F. Han, J. Zhu, L. Liu and A. Ge, Multilayer structured CNF/rGO aerogels and rGO film composites for efficient electromagnetic interference shielding, *Carbohydr. Polym.*, 2022, **286**, 119306.

68 H. Liu, Y. Xu, J.-P. Cao, D. Han, Q. Yang, R. Li and F. Zhao, Skin structured silver/three-dimensional graphene/polydimethylsiloxane composites with exceptional electromagnetic interference shielding effectiveness, *Composites, Part A*, 2021, **148**, 106476.

69 H. Zhang, G. Zhang, M. Tang, L. Zhou, J. Li, X. Fan, X. Shi and J. Qin, Synergistic effect of carbon nanotube and graphene nanoplates on the mechanical, electrical and electromagnetic interference shielding properties of polymer composites and polymer composite foams, *Chem. Eng. J.*, 2018, **353**, 381–393.

70 H. Liu, Y. Xu, X. Zhao, D. Han, F. Zhao and Q. Yang, Lightweight leaf-structured carbon nanotubes/graphene foam and the composites with polydimethylsiloxane for electromagnetic interference shielding, *Carbon*, 2022, **191**, 183–194.

71 T. Guo, X. Chen, L. Su, C. Li, X. Huang and X.-Z. Tang, Stretched graphene nanosheets formed the "obstacle walls" in melamine sponge towards effective electromagnetic interference shielding applications, *Mater. Des.*, 2019, **182**, 108029.

72 Z. Yu, T. Dai, S. Yuan, H. Zou and P. Liu, Electromagnetic Interference Shielding Performance of Anisotropic Polyimide/Graphene Composite Aerogels, *ACS Appl. Mater. Interfaces*, 2020, **12**, 30990–31001.

73 Y.-Y. Wang, W.-J. Sun, D.-X. Yan, K. Dai and Z.-M. Li, Ultralight carbon nanotube/graphene/polyimide foam with heterogeneous interfaces for efficient electromagnetic interference shielding and electromagnetic wave absorption, *Carbon*, 2021, **176**, 118–125.

74 Y. Li, M. Yu, P. Yang and J. Fu, Enhanced Microwave Absorption Property of Fe Nanoparticles Encapsulated within Reduced Graphene Oxide with Different Thicknesses, *Ind. Eng. Chem. Res.*, 2017, **56**, 8872–8879.

75 M. S. Cao, W. L. Song, Z. L. Hou, B. Wen and J. Yuan, The effects of temperature and frequency on the dielectric properties, electromagnetic interference shielding and microwave-absorption of short carbon fiber/silica composites, *Carbon*, 2010, **48**(3), 788–796.

76 Z. Jia, Z. Gao, K. Kou, A. Feng, C. Zhang, B. Xu and G. Wu, Facile synthesis of hierarchical A-site cation deficiency

perovskite LaxFeO3-y/RGO for high efficiency microwave absorption, *Compos. Commun.*, 2020, **20**, 100344.
77 X. Ren and G. Xu, Electromagnetic and microwave absorbing properties of NiCoZn-ferrites doped with La3+, *J. Magn. Magn. Mater.*, 2014, **354**, 44–48.
78 I. V. Zavislyak, M. A. Popov, E. D. Solovyova, S. A. Solopan and A. G. Belous, Dielectric-ferrite film heterostructures for magnetic field controlled resonance microwave components, *Mater. Sci. Eng. B*, 2015, **197**, 36–42.
79 T. Kagotani, R. Kobayashi, S. Sugimoto, K. Inomata, K. Okayama and J. Akedo, Magnetic properties and microwave characteristics of Ni–Zn–Cu ferrite film fabricated by aerosol deposition method, *J. Magn. Magn. Mater.*, 2005, **290–291**, 1442–1445.
80 M. Chahar, S. Dabas and O. P. Thakur, Enhanced electromagnetic shielding effectiveness of MWCNT/zinc-doped nickel ferrite nanocomposites, *Ceram. Int.*, 2022, **48**, 5352–5360.
81 S. Tyagi, R. C. Agarwala and V. Agarwala, Microwave Absorption and Magnetic Studies of Strontium Hexaferrites Nanoparticles Synthesized by Modified Flux Method, *J. Nano Res.*, 2010, **10**, 19–27.
82 R. Afrin, S. M. Abbas, N. A. Shah, M. F. Mustafa, Z. Ali and N. Ahmad, Effect of Varying Inert Gas and Acetylene Concentration on the Synthesis of Carbon Nanotubes, *J. Nanosci. Nanotechnol.*, 2016, **16**, 2956–2959.
83 S. Kumar, P. Kumar, R. Gupta and V. Verma, Electromagnetic interference shielding behaviors of in-situ polymerized ferrite-polyaniline nano-composites and ferrite-polyaniline deposited fabrics in X-band frequency range, *J. Alloys Compd.*, 2021, **862**, 158331.
84 F. Ren, D. Song, Z. Li, L. Jia, Y. Zhao, D. Yan and P. Ren, Synergistic Effect of Graphene Nanosheets and Carbonyl Iron–Nickel Alloy Hybrid Filler on Electromagnetic Interference Shielding and Thermal Conductivity of Cyanate Ester Composites, *J. Mater. Chem. C*, 2018, **6**, 1476.
85 X.-B. Zhou, L. Shen, L. Li, T.-M. Huang, C.-F. Hu, W.-M. Pan, X.-H. Jin, J. Sun, L. Gao and Q. Huang, Preparation of nanocrystalline-coated carbon nanotube/$Ni_{0.5}Zn_{0.5}Fe_2O_4$ composite with excellent electromagnetic property as microwave absorber, *J. Phys. D: Appl. Phys.*, 2013, **46**, 145002.
86 H. Wang, J. T. Robinson, G. Diankov and H. Dai, Nanocrystal Growth on Graphene with Various Degrees of Oxidation, *J. Am. Chem. Soc.*, 2010, **132**, 3270–3271.
87 M. Bibi, S. M. Abbas, N. Ahmad, B. Muhammad, Z. Iqbal, U. A. Rana and S. U.-D. Khan, Microwaves absorbing characteristics of metal ferrite/multiwall carbon nanotubes nanocomposites in X-band, *Composites, Part B*, 2017, **114**, 139–148.
88 S. Sutradhar, K. Mukhopadhyay, S. Pati, S. Das, D. Das and P. K. Chakrabarti, Modulated magnetic property, enhanced microwave absorption and Mössbauer spectroscopy of $Ni_{0.40}Zn_{0.40}Cu_{0.20}Fe_2O_4$ nanoparticles embedded in carbon nanotubes, *J. Alloys Compd.*, 2013, **576**, 126–133.
89 J. Zhang, R. Shu, C. Guo, R. Sun, Y. Chen and J. Yuan, Fabrication of nickel ferrite microspheres decorated multi-walled carbon nanotubes hybrid composites with enhanced electromagnetic wave absorption properties, *J. Alloys Compd.*, 2019, **784**, 422–430.
90 S. Kumar, R. Walia, A. Kumar and V. Verma, Hybrid structure of MWCNT/ferrite and GO incorporated composites for microwave shielding properties and their practical applications, *RSC Adv.*, 2021, **11**, 9775–9787.
91 C. H. Phan, M. Mariatti and Y. H. Koh, Electromagnetic interference shielding performance of epoxy composites filled with multiwalled carbon nanotubes/manganese zinc ferrite hybrid fillers, *J. Magn. Magn. Mater.*, 2016, **401**, 472–478.
92 R.-B. Yang, P. M. Reddy, C.-J. Chang, P.-A. Chen, J.-K. Chen and C.-C. Chang, Synthesis and characterization of Fe_3O_4/polypyrrole/carbon nanotube composites with tunable microwave absorption properties: Role of carbon nanotube and polypyrrole content, *Chem. Eng. J.*, 2016, **285**, 497–507.
93 M. O. Faruk, A. Ahmed, M. A. Jalil, M. T. Islam, A. M. Shamim, B. Adak, M. M. Hossain and S. Mukhopadhyay, Functional textiles and composite based wearable thermal devices for Joule heating: progress and perspectives, *Appl. Mater. Today*, 2021, **23**, 101025.
94 H. Gao, C. Wang, Z. Yang and Y. Zhang, 3D porous nickel metal foam/polyaniline heterostructure with excellent electromagnetic interference shielding capability and superior absorption based on pre-constructed macroscopic conductive framework, *Compos. Sci. Technol.*, 2021, **213**, 108896.
95 G. Zhou, L. Yao, Z. Xie, U. Kamran, J. Xie, F. Zhang, S.-J. Park and Y. Zhang, Controllable construction of CNT-Interconnected liquid metal networks for thermal management, *Composites, Part A*, 2023, **175**, 107743.
96 Z. Yang, Y. Zhang and B. Wen, Enhanced electromagnetic interference shielding capability in bamboo fiber@polyaniline composites through microwave reflection cavity design, *Compos. Sci. Technol.*, 2019, **178**, 41–49.
97 S. M. K. Thiagamani, N. Rajini, S. Siengchin, A. Varada Rajulu, N. Hariram and N. Ayrilmis, Influence of silver nanoparticles on the mechanical, thermal and antimicrobial properties of cellulose-based hybrid nanocomposites, *Composites, Part B*, 2019, **165**, 516–525.
98 T. Senthil Muthu Kumar, K. Senthilkumar, M. Ratanit, N. Rajini, N. Chanunpanich, N. Hariram, P. Pornwongthong and S. Siengchin, Influence of Titanium Dioxide Particles on the Filtration of 1,4-Dioxane and Antibacterial Properties of Electrospun Cellulose Acetate and Polyvinylidene Fluoride Nanofibrous Membranes, *J. Polym. Environ.*, 2021, **29**, 775–784.
99 A. Azam, Size-dependent antimicrobial properties of CuO nanoparticles against Gram-positive and -negative bacterial strains, *Int. J. Nanomed.*, 2012, 3527–3535.

100 C. Cazan, A. Enesca and L. Andronic, Synergic Effect of TiO2 Filler on the Mechanical Properties of Polymer Nanocomposites, *Polymers*, 2021, **13**, 2017.
101 S. Patil, A. K. Bharimalla, A. Mahapatra, J. Dhakane-Lad, A. Arputharaj, M. Kumar, A. S. M. Raja and N. Kambli, Effect of polymer blending on mechanical and barrier properties of starch-polyvinyl alcohol based biodegradable composite films, *Food Biosci.*, 2021, **44**, 101352.
102 K. Tamilarasi, P. Aji Udhaya and M. Meena, Enhancement on the electrical and optical behaviour of ZnFe2O4 nano particles via transition metal substitution, *Mater. Today Proc.*, 2022, **64**, 1671–1678.
103 A. M. El Sayed and W. M. Morsi, α-Fe2O3/(PVA + PEG) Nanocomposite films; synthesis, optical, and dielectric characterizations, *J. Mater. Sci.*, 2014, **49**, 5378–5387.
104 P. Rani, M. B. Ahamed and K. Deshmukh, Dielectric and electromagnetic interference shielding properties of carbon black nanoparticles reinforced PVA/PEG blend nanocomposite films, *Mater. Res. Express*, 2020, **7**, 064008.
105 T. T. V. Tran, D.-V. N. Vo, S. T. Nguyen and C. M. Vu, Silver nanowires decorated recycled cigarette filters based epoxy composites with high through-plane thermal conductivity and efficient electromagnetic interference shielding, *Composites, Part A*, 2021, **149**, 106485.
106 C.-W. Lee, C.-H. Lin, L.-Y. Wang and Y.-H. Lee, Developing sustainable and recyclable high-efficiency electromagnetic interference shielding nanocomposite foams from the upcycling of recycled poly(ethylene terephthalate), *Chem. Eng. J.*, 2023, **468**, 143447.
107 F. Ding, S. Zhang, X. Chen, R. Li and X. Ren, PET fabric treated with environmental-friendly phosphorus-based compounds for enhanced flame retardancy, thermal stability and anti-dripping performance, *Composites, Part B*, 2022, **235**, 109791.
108 S. Piao, Z. Jiang, S. Li, T. Park, Y. Kim, E. Lee, S. Lee, S. H. Paek, J. Oh, H.-J. Im, W. Zhang, K. Lee and Y. Piao, Recycled polyethylene terephthalate/FeCo@C/Silver nanowire/polyimide sandwich membrane for electrothermal heating and electromagnetic interference shielding, *J. Alloys Compd.*, 2024, **987**, 174256.
109 Z. Jiang, S. Piao, T. Park, S. Li, Y. Kim, E. Lee, C. Bae, Y. Lee, H. J. Im, J. Oh, Y. Piao and K. Lee, Multifunctional Ultrathin Recycled PET-Based Membrane for Electromagnetic Interference Shielding, Antibacterial and Thermal Management, *Adv. Mater. Interfaces*, 2024, **11**(14), DOI: 10.1002/admi.202301047.
110 Z. Du, K. Chen, Y. Zhang, Y. Wang, P. He, H.-Y. Mi, Y. Wang, C. Liu and C. Shen, Engineering multilayered MXene/electrospun poly(lactic acid) membrane with increscent electromagnetic interference (EMI) shielding for integrated Joule heating and energy generating, *Compos. Commun.*, 2021, **26**, 100770.
111 J. Gao, W. Li, H. Shi, M. Hu and R. K. Y. Li, Preparation, morphology, and mechanical properties of carbon nanotube anchored polymer nanofiber composite, *Compos. Sci. Technol.*, 2014, **92**, 95–102.
112 E. Mikinka and M. Siwak, Recent advances in electromagnetic interference shielding properties of carbon-fibre-reinforced polymer composites—a topical review, *J. Mater. Sci.: Mater. Electron.*, 2021, **32**, 24585–24643.
113 B. Armynah, R. Anugrahwidya and D. Tahir, Composite cassava starch/chitosan/Pineapple Leaf Fiber (PALF)/Zinc Oxide (ZnO): Bioplastics with high mechanical properties and faster degradation in soil and seawater, *Int. J. Biol. Macromol.*, 2022, **213**, 814–823.
114 L. Dai, C. Qiu, L. Xiong and Q. Sun, Characterisation of corn starch-based films reinforced with taro starch nanoparticles, *Food Chem.*, 2015, **174**, 82–88.
115 Y. Zhang, Q. Gao and S. Zhang, rGO/MXene sandwich-structured film at spunlace nonwoven fabric substrate: Application to EMI shielding and electrical heating, *J. Colloid Interface Sci.*, 2022, **614**, 194–204.
116 T. Liu, Z. Liu, Z. Zhou, S. Q. Shi, Y. Tan, H. Chen, X. Sun, H. Ni, S. Gong and J. Li, A high-performance, sustainable nacre-mimetic film with montmorillonite nanosheets crosslinked natural wood powders, *Ind. Crops Prod.*, 2023, **193**, 116202.
117 J. Yang, Y. C. Ching, C. H. Chuah, D. H. Nguyen and N.-S. Liou, Synthesis and characterization of starch/fiber-based bioplastic composites modified by citric acid-epoxidized palm oil oligomer with reactive blending, *Ind. Crops Prod.*, 2021, **170**, 113797.
118 X. Si, Q. Zhang, X. Guo, J. Yang, T. Zhao and Y. Zhang, Bioinspired Chestnut Burr-like Polyaniline: Achieving Superhydrophobicity and Excellent Microwave Transparency through Controlled Polymerization, *ACS Appl. Mater. Interfaces*, 2025, **17**, 9867–9878.
119 A. Sedighi, M. Montazer and S. Mazinani, Fabrication of electrically conductive superparamagnetic fabric with microwave attenuation, antibacterial properties and UV protection using PEDOT/magnetite nanoparticles, *Mater. Des.*, 2018, **160**, 34–47.
120 D. Liu, R. Qiang, Y. Du and Y. Wang, Prussian blue analogues derived magnetic FeCo alloy/carbon composites with tunable chemical composition and enhanced microwave absorption, *J. Colloid Interface Sci.*, 2018, **514**, 10–20.
121 S. Kumar, A. Ohlan, P. Kumar and V. Verma, Improved Electromagnetic Interference Shielding Response of Polyaniline Containing Magnetic Nano-ferrites, *J. Supercond. Novel Magn.*, 2020, **33**, 1187–1198.
122 Moditma and S. Annapoorni, FeCo/PANI composites as electromagnetic shields in the X-band: An understanding of the loss mechanisms, *Mater. Chem. Phys.*, 2024, **323**, DOI: 10.1016/j.matchemphys.2024.129599.
123 S. Quillard, G. Louarn, S. Lefrant and A. G. Macdiarmid, Vibrational analysis of polyaniline: A comparative study of leucoemeraldine, emeraldine, and pernigraniline bases, *Phys. Rev. B: Condens. Matter Mater. Phys.*, 1994, **50**, 12496–12508.

124 B. Wang, Q. Wu, Y. Fu and T. Liu, A review on carbon/magnetic metal composites for microwave absorption, *J. Mater. Sci. Technol.*, 2021, **86**, 91–109.
125 Z. Wu, K. Pei, L. Xing, X. Yu, W. You and R. Che, Enhanced Microwave Absorption Performance from Magnetic Coupling of Magnetic Nanoparticles Suspended within Hierarchically Tubular Composite, *Adv. Funct. Mater.*, 2019, **29**, 1901448.
126 J. Song, Y. Gao, G. Tan, Q. Man and Z. Wang, Comparative study of microwave absorption properties of Ni–Zn ferrites obtained from different synthesis technologies, *Ceram. Int.*, 2022, **48**, 22896–22905.
127 L. Wang, X. Li, Q. Li, X. Yu, Y. Zhao, J. Zhang, M. Wang and R. Che, Oriented Polarization Tuning Broadband Absorption from Flexible Hierarchical ZnO Arrays Vertically Supported on Carbon Cloth, *Small*, 2019, **15**, 1900900.
128 N. Liu, X. Zhang, Y. Dou, X. Yan and L. Yu, Design of carbon aerogels with variable surface morphology for electromagnetic wave absorption, *Carbon*, 2022, **200**, 271–280.
129 L. Lyu, H. Chai, K. Seong, C. Lee, J. Kang, W. Zhang and Y. Piao, Yeast-derived N-doped carbon microsphere/polyaniline composites as high performance pseudocapacitive electrodes, *Electrochim. Acta*, 2018, **291**, 256–266.
130 Y. Zhang, Z. Yang and B. Wen, An Ingenious Strategy to Construct Helical Structure with Excellent Electromagnetic Shielding Performance, *Adv. Mater. Interfaces*, 2019, **6**, 1900375.
131 P. Zhang, X. Han, L. Kang, R. Qiang, W. Liu and Y. Du, Synthesis and characterization of polyaniline nanoparticles with enhanced microwave absorption, *RSC Adv.*, 2013, **3**, 12694.
132 J. Yang, Q. Zhang, S. Liu, H. Zhang, W. Xie, P. Liu, M. Meng, S. Song, H. Guan and Y. Zhang, Template-free synthesize of PANI nanostructures: Modulating structure for enhanced dielectric characteristics and superior electromagnetic wave absorption, *Mater. Res. Bull.*, 2025, **181**, 113073.
133 B. Wang, Y. Ji, C. Mu, Y. Huo, J. Xiang, A. Nie, T. Xue, K. Zhai, Z. Liu and F. Wen, Well-controlled Core-shell structures based on Fe3O4 nanospheres coated by polyaniline for highly efficient microwave absorption, *Appl. Surf. Sci.*, 2022, **591**, 153176.
134 Q. Shang, H. Feng, K. Pan, N. Chen, L. Tan and J. Qiu, Modified sepiolite/BaLa0.5Fe11.5O19@polyaniline composites with superior microwave absorption properties, *J. Mater. Sci.: Mater. Electron.*, 2020, **31**, 8523–8535.
135 T.-H. Lee, G.-Y. Han, M.-B. Yi, H.-J. Kim, J.-H. Lee and S. Kim, Rapid Photoresponsive Switchable Pressure-Sensitive Adhesive Containing Azobenzene for the Mini-Light Emitting Diode Transfer Process, *ACS Appl. Mater. Interfaces*, 2021, **13**, 43364–43373.
136 J. Liu, M.-S. Cao, Q. Luo, H.-L. Shi, W.-Z. Wang and J. Yuan, Electromagnetic Property and Tunable Microwave Absorption of 3D Nets from Nickel Chains at Elevated Temperature, *ACS Appl. Mater. Interfaces*, 2016, **8**, 22615–22622.
137 H. Zhang, G. Zhang, Q. Gao, M. Tang, Z. Ma, J. Qin, M. Wang and J.-K. Kim, Multifunctional microcellular PVDF/Ni-chains composite foams with enhanced electromagnetic interference shielding and superior thermal insulation performance, *Chem. Eng. J.*, 2020, **379**, 122304.
138 C. Wang, H. Gao, D. Liang, S. Liu, H. Zhang, H. Guan, Y. Wu and Y. Zhang, Effective fabrication of flexible nickel chains/acrylate composite pressure-sensitive adhesives with layered structure for tunable electromagnetic interference shielding, *Adv. Compos. Hybrid Mater.*, 2022, **5**, 2906–2920.
139 Y. Zhang, M. Qiu, Y. Yu, B. Wen and L. Cheng, A Novel Polyaniline-Coated Bagasse Fiber Composite with Core–Shell Heterostructure Provides Effective Electromagnetic Shielding Performance, *ACS Appl. Mater. Interfaces*, 2017, **9**, 809–818.
140 R. Na, J. Liu, G. Wang and S. Zhang, Light weight and flexible poly(ether ether ketone) based composite film with excellent thermal stability and mechanical properties for wide-band electromagnetic interference shielding, *RSC Adv.*, 2018, **8**, 3296–3303.
141 H. Wang, G. Wang, W. Li, Q. Wang, W. Wei, Z. Jiang and S. Zhang, A material with high electromagnetic radiation shielding effectiveness fabricated using multi-walled carbon nanotubes wrapped with poly(ether sulfone) in a poly(ether ether ketone) matrix, *J. Mater. Chem.*, 2012, **22**, 21232–21237.
142 Y. Su, F. Zhou, X. Wei, D. Jing, X. Zhang and S. Zhang, Enhanced mechanical and electrical properties of carbon fiber/poly(ether ether ketone) laminates via inserting carbon nanotubes interleaves, *J. Appl. Polym. Sci.*, 2020, **137**, 48658.
143 D. G. Papageorgiou, I. A. Kinloch and R. J. Young, Mechanical properties of graphene and graphene-based nanocomposites, *Prog. Mater. Sci.*, 2017, **90**, 75–127.
144 V. P. Veedu, A. Cao, X. Li, K. Ma, C. Soldano, S. Kar, P. M. Ajayan and M. N. Ghasemi-Nejhad, Multifunctional composites using reinforced laminae with carbon-nanotube forests, *Nat. Mater.*, 2006, **5**, 457–462.
145 K. Yang, H. Mei, D. Han and L. Cheng, Enhanced electromagnetic shielding property of C/SiC composites via electrophoretically-deposited CNTs onto SiC coating, *Ceram. Int.*, 2018, **44**, 20187–20191.
146 L. Yang, W. Zheng, P. Zhang, J. Chen, W. B. Tian, Y. M. Zhang and Z. M. Sun, MXene/CNTs films prepared by electrophoretic deposition for supercapacitor electrodes, *J. Electroanal. Chem.*, 2018, **830–831**, 1–6.
147 A. Gupta, S. Varshney, A. Goyal, P. Sambyal, B. Kumar Gupta and S. K. Dhawan, Enhanced electromagnetic shielding behaviour of multilayer graphene anchored luminescent TiO2 in PPY matrix, *Mater. Lett.*, 2015, **158**, 167–169.
148 S. S. Chauhan, P. Verma, R. S. Malik and V. Choudhary, Thermomechanically stable dielectric composites based on poly(ether ketone) and $BaTiO_3$ with improved

electromagnetic shielding properties in X-band, *J. Appl. Polym. Sci.*, 2018, **135**, 46413.

149 B. Jiang, J. Luan, S. Qin, T. Wu, G. Wang and S. Zhang, Fabrication of very effective ferroferric oxide and multiwalled carbon nanotubes@polyetherimide/poly(ether ether ketone) electromagnetic interference shielding composites, *Polym. Compos.*, 2020, **41**, 3135–3143.

150 S. Li, Y. Jin, Z. Wang, Q. He, R. Chen, J. Wang, H. Wu, X. Zhao and J. Mu, Preparation and characterisation of nickel-plated carbon fibre/polyether ether ketone composites with high electromagnetic shielding and high thermal conductivity, *Colloid Polym. Sci.*, 2019, **297**, 967–977.

151 Y. Yang, M. C. Gupta, K. L. Dudley and R. W. Lawrence, A Comparative Study of EMI Shielding Properties of Carbon Nanofiber and Multi-Walled Carbon Nanotube Filled Polymer Composites, *J. Nanosci. Nanotechnol.*, 2005, **5**, 927–931.

152 S. Gong, Z. H. Zhu, M. Arjmand, U. Sundararaj, J. T. W. Yeow and W. Zheng, Effect of carbon nanotubes on electromagnetic interference shielding of carbon fiber reinforced polymer composites, *Polym. Compos.*, 2018, **39**(S2), DOI: **10.1002/pc.24084**.

153 R. Rohini, K. Verma and S. Bose, Interfacial Architecture Constructed Using Functionalized MWNT Resulting in Enhanced EMI Shielding in Epoxy/Carbon Fiber Composites, *ACS Omega*, 2018, **3**, 3974–3982.

154 L. Yu, Y. Zhu and Y. Fu, Waxberry-like carbon@polyaniline microspheres with high-performance microwave absorption, *Appl. Surf. Sci.*, 2018, **427**, 451–457.

155 A. Feng, M. Ma, Z. Jia, M. Zhang and G. Wu, Fabrication of $NiFe_2$ O_4 @carbon fiber coated with phytic acid-doped polyaniline composite and its application as an electromagnetic wave absorber, *RSC Adv.*, 2019, **9**, 25932–25941.

156 B. P. Singh, V. Choudhary, P. Saini and R. B. Mathur, Designing of epoxy composites reinforced with carbon nanotubes grown carbon fiber fabric for improved electromagnetic interference shielding, *AIP Adv.*, 2012, **2**, 022151.

157 X. Mi, N. Liang, H. Xu, J. Wu, Y. Jiang, B. Nie and D. Zhang, Toughness and its mechanisms in epoxy resins, *Prog. Mater. Sci.*, 2022, **130**, 100977.

158 M. F. Maqsood, M. A. A. Zubair, M. A. Raza, S. M. Z. Mehdi, N. Lee, Z. U. Rehman, K. Park, M. U. Bhatti, U. Latif and A. Tawakkal, Fabrication and characterization of graphene oxide and glass fiber-based hybrid epoxy composites, *Polym. Compos.*, 2022, **43**, 8072–8083.

159 D. D. L. Chung, Electromagnetic interference shielding effectiveness of carbon materials, *Carbon*, 2001, **39**, 279–285.

160 J.-B. Donnet and R. Chand Bansal, *Carbon Fibers*, CRC Press, 0 edn, 1998.

161 X. Jia, Y. Li, B. Shen and W. Zheng, Evaluation, fabrication and dynamic performance regulation of green EMI-shielding materials with low reflectivity: A review, *Composites, Part B*, 2022, **233**, 109652.

162 R. Moučka, M. Sedlačík, J. Prokeš, H. Kasparyan, S. Valtera and D. Kopecký, Electromagnetic interference shielding of polypyrrole nanostructures, *Synth. Met.*, 2020, **269**, 116573.

163 H. Chen, X. Cai and X. Bi, The influence of polypyrrole coating on the mechanical properties of carbon fiber-filled polytetrafluoroethylene composite, *J. Thermoplast. Compos. Mater.*, 2014, **27**, 1065–1073.

164 J. Yan, Y. Huang, X. Liu, X. Zhao, T. Li, Y. Zhao and P. Liu, Polypyrrole-Based Composite Materials for Electromagnetic Wave Absorption, *Polym. Rev.*, 2021, **61**, 646–687.

165 A. A. Khodiri, M. Y. Al-Ashry and A. G. El-Shamy, Novel hybrid nanocomposites based on polyvinyl alcohol/graphene/magnetite nanoparticles for high electromagnetic shielding performance, *J. Alloys Compd.*, 2020, **847**, 156430.

166 S. Ata, S. A. Bukhari, I. Bibi, I. Mohsin, M. Shoaib, F. Majid, M. Iqbal, F. H. Alshammari, N. Alfryyan and N. Alwadai, Magnetite/graphene oxide/Prussian blue composite with robust effectiveness for electromagnetic interference shielding, *Ceram. Int.*, 2022, **48**, 1690–1698.

167 A. S. Teja and P.-Y. Koh, Synthesis, properties, and applications of magnetic iron oxide nanoparticles, *Prog. Cryst. Growth Charact. Mater.*, 2009, **55**, 22–45.

168 F. C. D. Reis, N. A. S. Gomes, M. R. Baldan, B. Ribeiro and M. C. Rezende, The influence of carbonyl iron and magnetite ferrite on the electromagnetic behavior of nanostructured composites based on epoxy resin/buckypapers, *J. Magn. Magn. Mater.*, 2022, **563**, 170007.

169 M. F. Shakir, A. N. Khan, R. Khan, S. Javed, A. Tariq, M. Azeem, A. Riaz, A. Shafqat, H. M. Cheema, M. A. Akram, I. Ahmad and R. Jan, EMI shielding properties of polymer blends with inclusion of graphene nano platelets, *Results Phys.*, 2019, **14**, 102365.

170 M. Verma, S. S. Chauhan, S. K. Dhawan and V. Choudhary, Graphene nanoplatelets/carbon nanotubes/polyurethane composites as efficient shield against electromagnetic polluting radiations, *Composites, Part B*, 2017, **120**, 118–127.

171 F. Majid, M. D. Ali, S. Ata, I. Bibi, A. Malik, A. Ali, N. Alwadai, H. Albalawi, M. Shoaib, S. A. Bukhari and M. Iqbal, Fe3O4/graphene oxide/Fe4[Fe(CN)6]3 nanocomposite for high performance electromagnetic interference shielding, *Ceram. Int.*, 2021, **47**, 11587–11595.

172 J. Wang, C. Xiang, Q. Liu, Y. Pan and J. Guo, Ordered Mesoporous Carbon/Fused Silica Composites, *Adv. Funct. Mater.*, 2008, **18**, 2995–3002.

173 K. S. Anu, K. A. Vishnumurthy, A. Mahesh and K. Natarajan, Carbon fiber-reinforced, activated carbon-embedded copper oxide nanoparticles/epoxy hybrid composites for EMI shielding in aircraft applications, *Polym. Bull.*, 2024, **81**, 8723–8750.

174 M. Raimondo, C. Naddeo, L. Vertuccio, K. Lafdi, A. Sorrentino and L. Guadagno, Carbon-Based Aeronautical Epoxy Nanocomposites: Effectiveness of

Atomic Force Microscopy (AFM) in Investigating the Dispersion of Different Carbonaceous Nanoparticles, *Polymers*, 2019, **11**, 832.

175 *Aerospace Materials and Applications*, ed. B. N. Bhat, American Institute of Aeronautics and Astronautics, Inc., Reston ,VA, 2018.

176 X. Huang, B. Dai, Y. Ren, J. Xu and P. Zhu, Preparation and Study of Electromagnetic Interference Shielding Materials Comprised of Ni-Co Coated on Web-Like Biocarbon Nanofibers via Electroless Deposition, *J. Nanomater.*, 2015, **2015**, 320306.

177 A. A. Al-Ghamdi and F. El-Tantawy, New electromagnetic wave shielding effectiveness at microwave frequency of polyvinyl chloride reinforced graphite/copper nanoparticles, *Composites, Part A*, 2010, **41**, 1693–1701.

178 P. Rani, M. B. Ahamed and K. Deshmukh, Significantly enhanced electromagnetic interference shielding effectiveness of montmorillonite nanoclay and copper oxide nanoparticles based polyvinylchloride nanocomposites, *Polym. Test.*, 2020, **91**, 106744.

179 J. Li, P. Zhao, M. Jing, X. Luo, J. Guo and F. Zhang, Enhanced Microwave Deicing Capacity of Cement Pavement with Carbon Fiber Screens, *Materials*, 2024, **17**, 1488.

180 T. Hanaoka, H. Ikematsu, S. Takahashi, N. Ito, N. Ijuin, H. Kawada, Y. Arao and M. Kubouchi, Recovery of carbon fiber from prepreg using nitric acid and evaluation of recycled CFRP, *Composites, Part B*, 2022, **231**, 109560.

181 K. Kawajiri and M. Kobayashi, Cradle-to-Gate life cycle assessment of recycling processes for carbon fibers: A case study of ex-ante life cycle assessment for commercially feasible pyrolysis and solvolysis approaches, *J. Cleaner Prod.*, 2022, **378**, 134581.

182 Y. Yao, F. Zhao, B. Wang, Z. Hu and Y. Huang, The designing of degradable unsaturated polyester based on selective cleavage activated hydrolysis and its application in recyclable carbon fiber composites, *Compos. Sci. Technol.*, 2022, **229**, 109692.

183 K. Wang, W. Chu, Y. Chen, H. Li and H. Liu, Maintaining electromagnetic interference shielding and flame-retardant performance of recycled carbon fiber-reinforced composites under multiple pyrolysis recycles, *Compos. Sci. Technol.*, 2024, **248**, DOI: 10.1016/j.compscitech.2024.110470.

184 H. Cheng, L. Guo, L. Zheng, Z. Qian and S. Su, A closed-loop recycling process for carbon fiber-reinforced polymer waste using thermally activated oxide semiconductors: Carbon fiber recycling, characterization and life cycle assessment, *Waste Manage.*, 2022, **153**, 283–292.

185 H. Cheng, L. Guo, Z. Qian, R. Sun and J. Zhang, Remanufacturing of recycled carbon fiber-reinforced composites based on fused deposition modeling processes, *Int. J. Adv. Manuf. Technol.*, 2021, **116**, 1609–1619.

186 K. Wang, C. Chen, Q. Zheng, J. Xiong, H. Liu, L. Yang, Y. Chen and H. Li, Multifunctional recycled carbon fiber-Ti3C2Tx MXene paper with superior electromagnetic interference shielding and photo/electro-thermal conversion performances, *Carbon*, 2022, **197**, 87–97.

187 X. Huan, K. Shi, J. Yan, S. Lin, Y. Li, X. Jia and X. Yang, High performance epoxy composites prepared using recycled short carbon fiber with enhanced dispersibility and interfacial bonding through polydopamine surface-modification, *Composites, Part B*, 2020, **193**, 107987.

188 J. Chen, K. Zhang, K. Zhang, B. Jiang and Y. Huang, Facile preparation of reprocessable and degradable phenolic resin based on dynamic acetal motifs, *Polym. Degrad. Stab.*, 2022, **196**, 109818.

189 Z. Deng, J. Fan, Z. Huang and X. Yang, Efficient recycling of carbon fiber from carbon fiber reinforced composite and reuse as high performance electromagnetic shielding materials with superior mechanical strength, *Polym. Test.*, 2023, **125**, 108110.

190 H. Zheng, W. Zhang, B. Li, J. Zhu, C. Wang, G. Song, G. Wu, X. Yang, Y. Huang and L. Ma, Recent advances of interphases in carbon fiber-reinforced polymer composites: A review, *Composites, Part B*, 2022, **233**, 109639.

191 S. E. Adler, B. E. Güttler, L. Bendler and K. Friedrich, Evaluation of recycled carbon fibre/epoxy composites: Thermal degradation behaviour of pyrolysed and virgin carbon fibres using thermogravimetric analysis, *Adv. Ind. Eng. Polym. Res.*, 2021, **4**, 82–92.

192 L. Guo, L. Xu, Y. Ren, Z. Shen, R. Fu, H. Xiao and J. Liu, Research on a two-step pyrolysis-oxidation process of carbon fiber-reinforced epoxy resin-based composites and analysis of product properties, *J. Environ. Chem. Eng.*, 2022, **10**, 107510.

193 Y. Lu, X. Zhao, Y. Lin, P. Li, Y. Tao, Z. Wang, J. Ma, H. Xu and Y. Liu, Lightweight MXene/carbon composite foam with hollow skeleton for air-stable, high-temperature-resistant and compressible electromagnetic interference shielding, *Carbon*, 2023, **206**, 375–382.

194 F. Hu, X. Wang, S. Bao, L. Song, S. Zhang, H. Niu, B. Fan, R. Zhang and H. Li, Tailoring electromagnetic responses of delaminated Mo2TiC2T MXene through the decoration of Ni particles of different morphologies, *Chem. Eng. J.*, 2022, **440**, 135855.

195 P. Rani Agarwal, R. Kumar, S. Kumari and S. R. Dhakate, Three-dimensional and highly ordered porous carbon–MnO2 composite foam for excellent electromagnetic interference shielding efficiency, *RSC Adv.*, 2016, **6**(103), 100713–100722.

196 A. Muzaffar, M. B. Ahamed, K. Deshmukh and S. K. K. Pasha, Dielectric properties and electromagnetic interference shielding studies of nickel oxide and tungsten oxide reinforced polyvinylchloride nanocomposites, *Polym.-Plast. Technol. Mater.*, 2020, **59**, 1667–1678.

197 Y. Song, F. Yin, C. Zhang, W. Guo, L. Han and Y. Yuan, Three-Dimensional Ordered Mesoporous Carbon Spheres Modified with Ultrafine Zinc Oxide Nanoparticles for Enhanced Microwave Absorption Properties, *Nano-Micro Lett.*, 2021, **13**, 76.

198 L. Song, C. Wu, Q. Zhi, F. Zhang, B. Song, L. Guan, Y. Chen, H. Wang, R. Zhang and B. Fan, Multifunctional SiC aerogel reinforced with nanofibers and nanowires for high-efficiency electromagnetic wave absorption, *Chem. Eng. J.*, 2023, **467**, 143518.

199 L. Song, B. Fan, Y. Chen, Q. Gao, Z. Li, H. Wang, X. Zhang, L. Guan, H. Li and R. Zhang, Ultralight and hyperelastic SiC nanofiber aerogel spring for personal thermal energy regulation, *J. Adv. Ceram.*, 2022, **11**, 1235–1248.

200 V. K. Patle, Y. Mehta and R. Kumar, Nickel and iron nanoparticles decorated carbon fibers reinforced phenolic resin-based carbon composites foam for excellent electromagnetic interference shielding, *Diamond Relat. Mater.*, 2024, **145**, DOI: 10.1016/j.diamond.2024.111069.

201 K. Ji, H. Zhao, J. Zhang, J. Chen and Z. Dai, Fabrication and electromagnetic interference shielding performance of open-cell foam of a Cu–Ni alloy integrated with CNTs, *Appl. Surf. Sci.*, 2014, **311**, 351–356.

202 Z. Fan, D. Wang, Y. Yuan, Y. Wang, Z. Cheng, Y. Liu and Z. Xie, A lightweight and conductive MXene/graphene hybrid foam for superior electromagnetic interference shielding, *Chem. Eng. J.*, 2020, **381**, 122696.

203 H.-G. Shi, H.-B. Zhao, B.-W. Liu and Y.-Z. Wang, Multifunctional Flame-Retardant Melamine-Based Hybrid Foam for Infrared Stealth, Thermal Insulation, and Electromagnetic Interference Shielding, *ACS Appl. Mater. Interfaces*, 2021, **13**, 26505–26514.

204 H. Liu, J. Wu, Q. Zhuang, A. Dang, T. Li and T. Zhao, Preparation and the electromagnetic interference shielding in the X-band of carbon foams with Ni-Zn ferrite additive, *J. Eur. Ceram. Soc.*, 2016, **36**, 3939–3946.

205 S. Farhan, R. Wang and K. Li, Carbon foam decorated with silver particles and in situ grown nanowires for effective electromagnetic interference shielding, *J. Mater. Sci.*, 2016, **51**, 7991–8004.

206 F. Qi, L. Wang, Y. Zhang, Z. Ma, H. Qiu and J. Gu, Robust Ti3C2Tx MXene/starch derived carbon foam composites for superior EMI shielding and thermal insulation, *Mater. Today Phys.*, 2021, **21**, 100512.